Environmental Modelling and Software 169 (2023) 105830

Contents lists available at ScienceDirect

Environmental Modelling and Software

journal homepage: www.elsevier.com/locate/envsoft

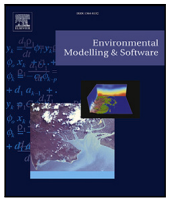

Analysis and comparison of coupled and uncoupled simulations with the COAWST model during the Gloria Storm (January 2020) in the northwestern Mediterranean Sea

Jordi Iglesias [a,*], Ildefonso Cuesta [a], Clara Salueña [a], Jordi Moré [b], Jordi Solé [c]

[a] Universitat Rovira i Virgili, Av. Països Catalans, 26, Tarragona, 43007, Spain
[b] Servei Meteorològic de Catalunya, Barcelona, Spain
[c] Department of Ocean and Earth Dynamics, Universitat de Barcelona, Barcelona, Spain

ARTICLE INFO

Keywords:
COAWST
NW Mediterranean
Gloria Storm
Balearic sea
Catalonia

ABSTRACT

Numerical simulations of the ocean and atmosphere provide crucial information for climate policies and socio-economic decisions. A coupled atmosphere–ocean model can potentially improve the representation of processes and forecast fields compared to an uncoupled one. This work aims to assess under which conditions the coupled model performs better than the uncoupled one and evaluate those differences in a high-energy storm in the northwestern Mediterranean area, which was modeled to compare coupled and uncoupled simulations of storm Gloria (January 2020). The model was validated and verified with observations from weather stations, atmospheric soundings, buoys, and the operational models of METEOCAT. Although the coupling of the models does not substantially affect the atmospheric large-scale flows, a significant impact has been found for the small and mesoscale structures. On the ocean, differences between the coupled and uncoupled models arise over the entire spatial and temporal scales, which the coupling exhibits better performance.

Software availability

Name of the software: COAWST: A Coupled-Ocean-Atmosphere-Wave-Sediment Transport Modeling System
Version: 3.6
Coupler: - Model Coupling Toolkit (MCT) v 2.6.0
Ocean: - Regional Ocean Modeling System (ROMS) 3.8 svn 1013
Atmosphere: - Weather Research and Forecasting Model (WRF) v 4.1.2
Wave(s): - Simulating Waves Nearshore (SWAN) v 41.31
Software availability: https://github.com/jcwarner-usgs/COAWST
Release Date: April 23, 2020
User Forums:
MCT http://www.mcs.anl.gov/research/projects/mct/
ROMS https://www.myroms.org/forum/index.php
WRF http://forum.wrfforum.com/
SWAN http://swanmodel.sourceforge.net/

1. Introduction

The frequency of extreme weather events has increased in recent years. This is widely attributed to anthropogenic climate change and is one of the most serious future threats (Ornes, 2018). Moreover, society is becoming more and more dependent on commodities such as electrical devices, transport and air conditioning. This, combined with the increasing adoption of electric cars, is leading to an increase in energy demand.

Additionally, the recent socio-economic situation of energy crisis demands additional efforts in the use of renewable energies (Delbeke, 2022), Therefore, the accuracy of atmospheric and ocean simulations represents a critical factor that will allow the achievement of significant advances in a plethora of areas, like the optimization of wind farm placements for a maximum energy extraction, the impact of wind turbines on the atmospheric conditions and their surroundings, the prediction of temperatures and pollutant dispersion, among many others (María Palomares et al., 2016; Mughal et al., 2017). A clear example of this was the simulation of the sulphur dioxide cloud emitted by Cumbre Vieja volcano (Canary Islands, Spain), conducted by the Copernicus Atmospheric Monitoring Service. This allowed the definition of the potentially-affected areas and the subsequent application of protective measures for both the local population and fauna (ECMWF, 2022).

* Corresponding author.
E-mail addresses: jordi.iglesias@urv.cat (J. Iglesias), ildefonso.cuesta@urv.cat (I. Cuesta), clara.saluena@urv.cat (C. Salueña), jordi.more@gencat.cat (J. Moré), jordi.sole@ub.edu (J. Solé).

https://doi.org/10.1016/j.envsoft.2023.105830
Received 7 December 2022; Received in revised form 9 September 2023; Accepted 14 September 2023
Available online 22 September 2023

Researchers have been working to develop better tools such as methodologies, approximations, modeling systems and software. The Coupled-Ocean-Atmosphere-Wave-Sediment Transport (COAWST) model (Warner et al., 2010) is the coupling of the atmospheric model, Weather Research and Forecasting (WRF), the wave model, Simulating WAves Nearshore (SWAN), and the ocean model, Regional Ocean Modeling System (ROMS). These models have been widely used in the last decades, and they are fully studied. Each of them uses lower resolution data than the model itself to define the boundary conditions and solves the Navier–Stokes equations considering a large number of parameterizations to take into account the effects of the smaller scales. This way they can provide an accurate approximation of the flow dynamics in the study area. The COAWST model allows the communication of the outputs of each model with the others, as well as the current feedback. This model has been employed in many studies, for instance, to reproduce hurricanes (Zambon et al., 2014), to study the wave–current interaction (Barbariol et al., 2013) and the two-way coupling. Other works address how to optimize the coupling parameters to avoid overestimations or underestimations of the current feedback to the atmosphere (Renault et al., 2020). In some cases and depending on the configuration, the coupling does not produce a beneficial effect, mainly because it is a sink of energy from mesoscale currents to the atmosphere (Renault et al., 2017). Nevertheless, they propose a wind adjustment. Other researchers have found that the full-coupling entails a benefit and is the most skilful simulation (Renault et al., 2012; Nicholls and Decker, 2015).

Considering all the previously-cited research, the main objective of the study is to evaluate the differences between the coupled and uncoupled simulations for each model (WRF, ROMS, and SWAN) during a high-energy storm. The comparison includes multiple important fields in the three models. Overall, the study aims not only to determine which simulation (coupled or decoupled) is the best but mainly focuses on studying the differences obtained in the simulations when using all three models coupled versus running them separately. In the latter case, the atmospheric model is first calculated, and the prognostic fields obtained are used to force the wave and ocean models. However, in cases where experimental data are available (weather stations, buoys, moorings, sounding and satellite), it has been established and commented on which of the two simulations fits the experimental data better. The goal is to provide information on these differences to help other researchers choose the model that best suits their needs which is key for future research or applied projects since it provides knowledge on the advantages/disadvantages and performance of each approach.

The Gloria Storm (January 2020) was one of the most intense atmospheric and ocean events since 1982 in the Mediterranean Sea. As it is a relatively recent event, not much literature is available, and Amores et al. (2020), De Alfonso et al. (2021) are works in which this storm was studied. Storm Gloria started as a developing complex of low-pressure systems over the central United States on January 9. The strongest system was named Winter Storm Isaiah by The Weather Channel. It brought severe thunderstorms and tornadoes to the south-central United States on January, 10. Isaiah continued to intensify as it moved eastwards across the United States before exiting into the north Atlantic on January, 13. After stalling off the coast of North America, the system was named Cyclone Ilka on January, 17. It moved steadily eastwards across the open Atlantic and approached the Iberian Peninsula. On January, 19, the storm made landfall near Santander in northern Spain as Storm Gloria. It passed over northern Spain as a weak cyclone, then entered the western Mediterranean Sea where it stalled for several days. After remaining near the Balearic Islands for about 48 h, Gloria slowly drifted southwards and westwards. It passed over the Strait of Gibraltar and northern Morocco on January, 22 before emerging into the far eastern Atlantic on January, 23. The storm looped offshore to the south and west of Portugal before dissipating on January 25 off the country's southern coast. Fig. 13 shows the significant wave height at different locations and can provide visual support to demonstrate the temporal variation in storm intensity.

This article uses the Gloria Storm for studying the impact of the coupling between models. The relevance of studying such extreme meteorological phenomena stems from the fact that climate models show an increased frequency not only in storms like Gloria but also cyclones, heat and cold waves (IPCC, 2022). Because of their human, ecological and socio-economic impact, the optimization of the currently-available tools for the prediction of these events is a priority.

This work starts with a brief model explanation, the study area, the boundary and forcing conditions, and the validation of the model. This validation was conducted using the operational model outputs generated at the Meteorological Service of Catalonia (METEOCAT[1]), as well as data from meteorological stations and buoys. The results of the coupled and non-coupled approaches involve the study of multiple fields of each model. Wind velocity, air temperature, relative humidity and temporal divergence are studied in the atmosphere. In the ocean, the currents, temperature, salinity and thermocline are compared, while significant wave height is obtained in the wave model.

2. Materials and methods

2.1. Area of study

The area of study is located in the northwestern Mediterranean Sea (Fig. 1). This area has a great variety of different geographical features, such as the Pyrenees and the Balearic Islands (Peña et al., 2011).

The two main rivers of this area were modeled in this study: *Ebro* and the *Rhône* with an average flow rate, from 17th to 25th of 491 m^3/s and 1341 m^3/s respectively. Just below the Gulf of Lion, the western end of the North Balearic front reaches the Pyrenean axis. In this area, the continental shelf is narrow (3 to 11 miles on average) and crossed by submarine canyons. The shelf-slope front separates waters of different densities between the continental shelf and the open sea. This front favors the narrowing of the northern current, which comes from the Gulf of Lion when it reaches the Catalan coast and circulates in a southwesterly direction along the continental shelf. In this space, there are two differentiated divergence zones, one towards the point 42°N, 4°E and the other around the point 41°N, 3°E (Pinot et al., 1995; Millot, 1999).

The combination of these characteristics, along with a favorable balance between sea and land points, makes the selected study area ideal for the objectives of this work. Allowing to see how the differences caused by the coupling propagate into land areas.

2.1.1. Domain analysis in zones

The characteristics of the domain were analyzed and it was found to have a good balance between sea and land areas, so the results could be applied to another domain with similar conditions. The effect of coupling was evaluated by dividing the domain into zones and analyzing the differences in the forecast fields at sea, near the coast, and land. A cell (i, j) was considered "sea" (or "land") if it and the 120 cells surrounding it in a stencil ranging from $(i-5, j-5)$ to $(i+5, j+5)$ are also sea (or land). Otherwise, it was classified as coast (Fig. 2).

To carry out an exhaustive analysis, the land and coastal areas were divided into different heights. This implied a different number of cells for comparison. The case of the coastal regions with high altitudes was eliminated so as not to unbalance the sampling.

In the ROMS ocean model, different criteria were defined for the division into zones. In some studies, the domain was divided according to certain relevant physical variables, e.g. Coriolis factor divided

[1] METEOCAT is a public company attached to the *Department of Climate Action, Food and Rural Agenda of the Government of Catalonia*, in charge of managing the weather observation and forecasting systems in Catalonia.

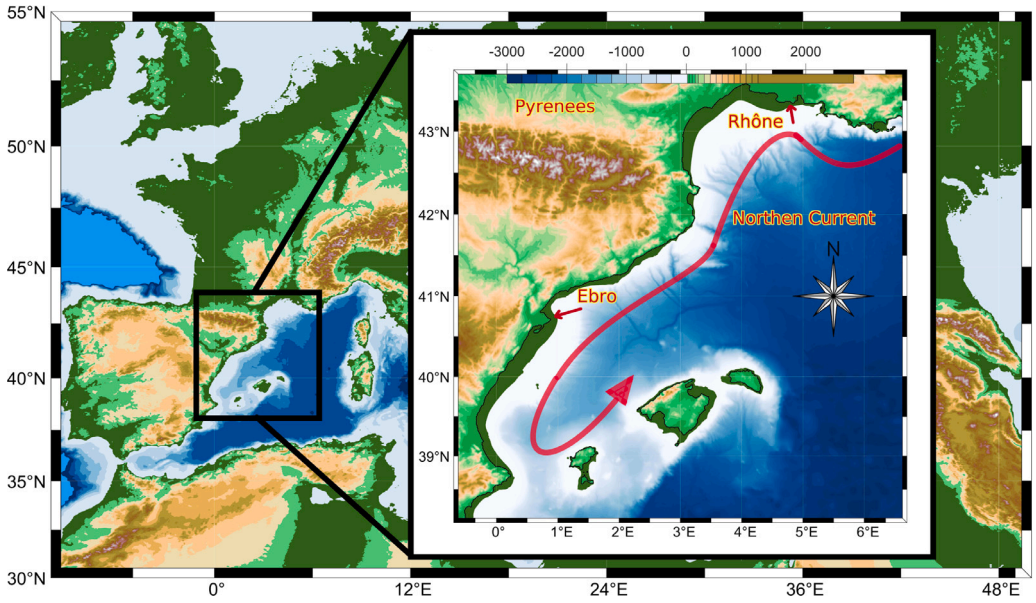

Fig. 1. Domain in the northwestern Mediterranean Sea used in the simulations. Bathymetry and orography are given in meters, longitude and latitude in degrees North and East.

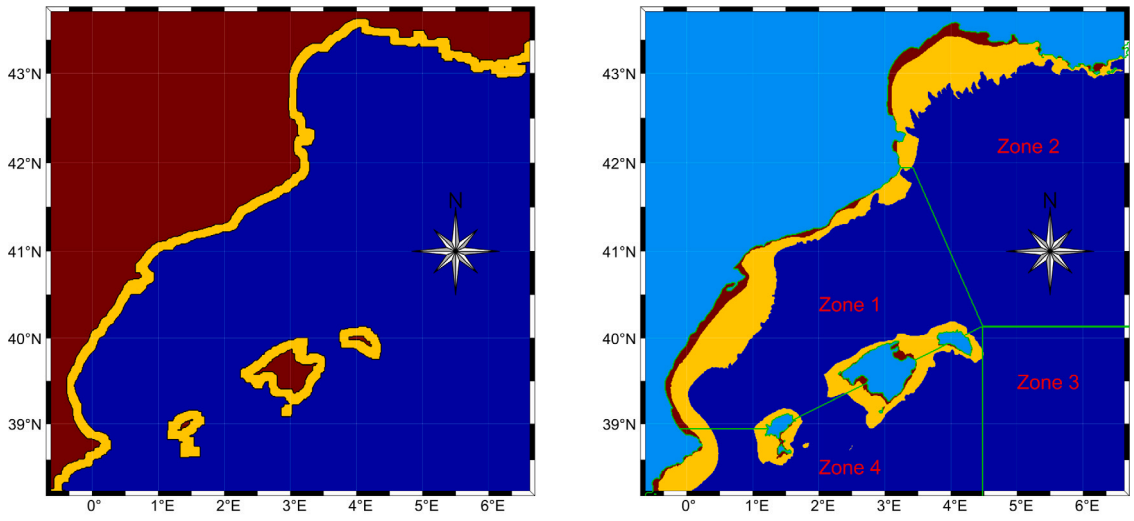

(a) WRF zones (b) ROMS zones

Fig. 2. Spatial division of the domain into different zones, (a) red = land, light brown=coast and dark blue = sea, (b) Contours of the bathymetrical based classification, soft blue = land, magenta =< 50 m, light brown = 50 to 200 m and dark blue => 200 m. and division per zones according to oceanographical criteria is also presented.

by height (Clavel-Henry et al., 2019) or seawater density anomalies (Clavel-Henry et al., 2021). The historical CMEMS model data was analyzed, and after calculating the temporal mean current from 1993 to 2020, the ocean mixed layer thickness density from 1993 to 2020, and the wind magnitude from 2000 to 2021 from the ERA5 model, it was concluded that four characteristic zones could be distinguished (Fig. 2(b)). Zone 1 extended from the coast of Catalonia to the Balearic Islands, zone 2 from the Gulf of Lion to Menorca Island, zone 3 is the square bounded by the domain limits and Menorca, and zone 4 is located at the south of the archipelago.

An additional analysis based on the depth of the sea in each particular point was performed (Fig. 2), The domain was divided into 3 sections: from the free surface to 50 m, between the 50 m and 200 m, and more than 200 m. The whole domain difference of the studied variables was analyzed and plotted as well, showing the same behavior and values deeper than 200 m. This is because the number of cells in this last case is much bigger than in the others.

2.2. Models

The coupled Ocean-Atmosphere-Wave-Sediment Transport Modeling System (COAWST) (Warner et al., 2010) was used for the comparison of coupled and uncoupled simulations during the Gloria Storm. The models in the COAWST system are, Weather Research and Forecasting (WRF) for the atmosphere, Regional Ocean Modeling System (ROMS) for the ocean, and Simulation WAves Nearshore (SWAN) for wave simulation. The Model Coupling Toolkit is used to transform and send data between models. The WRF, ROMS, and SWAN models are also used without coupling for comparison (See Section 5.1 for more details).

The three domains were developed following Renault et al. (2020) recommendations. the domains have approximately 1 km × 1 km regular spatial grid resolution and are the same in the 3 models to avoid interpolating the fields. Therefore, the differences between coupled and uncoupled simulations lie solely in the methodology and are not

magnified or reduced by the interpolation method (see Section 5.2 for more details about the model set-up). Solbakken et al. (2021) show that 1 km simulations tend to better reproduce the mean wind features in complex terrains.

The model gives consistent and valid results for time steps of 6 s for WRF and ROMS, and 12 s for SWAN. The spin-up time of the model had been established in 48 h based on autocorrelations of the monitored variables (wind components, temperatures, etc.).

2.2.1. Boundary and initial conditions

The ERA5 model, the fifth generation ECMWF reanalysis is used for creating the required WRF fields, the used data being hourly pressure levels from 1979 to the present as well as single levels with a resolution of 0.25° × 0.25°. The vertical coverage is from 1000 hPa to 1 hPa in 37 levels and the data are in GRIB format, in the coupled simulation, the sea surface temperatures are exchanged with ROMS. In the case of WRF without coupling, the sea surface temperature is manually implemented using the same hourly instantaneous data used to feed the initial and forcing conditions in ROMS. All of these data are incorporated through the WRF Preprocessing System (WPS), except the sea surface temperature.

ROMS model data were obtained from the Mediterranean Sea model of the Copernicus Marine Service CMEMS.[2] The physical component of the Mediterranean Forecasting System (Med-Currents) is a coupled hydrodynamic-wave model for the Mediterranean basin, including tides. The model's horizontal grid resolution is 1/24° (≈4.5 km) and has 141 unevenly spaced vertical levels. The ROMS inputs, which include temperature, current velocities (U and V), sea surface height, and salinity, have been processed. Firstly, horizontal interpolation was performed at each of the 141 vertical levels, and then vertical interpolation was conducted towards the 40 rho points. These data are not publicly available, a request was made to CMEMS (Copernicus Marine Environment Monitoring Service) to obtain the hourly data for these five fields. The tides were obtained from OSU Tidal Prediction Software.

For SWAN, in coupled simulation, the forcing is provided by the WRF model for wind and the ROMS model for currents. However, in non-coupled simulation, the forcing is derived from the post-processed wind outputs of the WRF model.

2.2.2. Model data intercomparison

To verify the COAWST simulations, the results were compared with the operational outputs generated at METEOCAT during the Gloria storm (Le Roux et al., 2018). The domain and parameterizations are similar, but it is important to note that both models are not directly comparable, because the mesh is different. METEOCAT uses a nested mesh, with the finest resolution of 3 km. Then, the mesh of 1 km resolution was interpolated to the METEOCAT mesh by means of Matlab scattered interpolant (Amidror, 2002; Ekström, 2016) for evaluation of both outputs.

Due to a smaller mesh size (–1 km instead of 3 km), smaller structures can be observed in our simulation. In addition to this, a smaller time step allows the observation of Von Kármán vortex structures past the mountains. Since a detailed description of these phenomena would be excessive for our purposes, the following fields were selected for quantitative analysis: temperature, velocity components, and vorticity. The velocity and vorticity images show similarities in large-scale structures, as opposed to small-scale structures, with variations caused mainly by differences in grid resolution and time step.

[2] (https://resources.marine.copernicus.eu/product-detail/MEDSEA_MULTIYEAR_PHY_006_004/INFORMATION)

2.2.3. Experimental data comparison

The results of both simulations have been compared with each other and with the automatic weather stations of the Catalan XEMA,[3] which provide 183 points for temperature measurement at 2 m and 92 for wind speed measurement at 10 m (https://es.meteocat.gencat.cat/xema). Station data are available every 30 min, as are the model outputs. The ROMS and SWAN ocean data were compared with hourly data from the 7 mooring buoys that *Puertos del Estado*[4] has in the study area. Additionally, data series were obtained from the 18 ARGO buoys operating in the area during the Gloria storm. Unfortunately, most of the buoy data were found to be useless or missing, so due to this unforeseen inconvenience, only the data from one buoy was used as supplementary material (See Fig. 16). The location of this buoy was (39.9752N, 5.1555E) on January 23, 2020 at 5:45 AM, its height was calculated using Eq. (3.32.3) from Commission et al. (2015). The data series was compared with the results of the simulations at 6:00 AM. In addition, the atmospheric sounding of Barcelona (from METEOCAT) with latitude 41.3844°N and longitude 2.1181°E was used to validate the vertical profiles of temperature and velocity. The data is available every 12 h. The location of this experimental data is shown in Fig. 3.

2.2.4. SWAN wavelets

SWAN analysis showed some major differences when compared to the other models, which will be described in a later section. A contour plot of the results allowed the distinction of the small scales of the flow. To study them, wavelet analysis was used instead of a Fourier because no information is lost during the deconstruction or reconstruction process (Nakken, 1999). A series of techniques for the application of wavelets in atmospheric sciences can be found in Domingues et al. (2005). For signal deconstruction, Daubechies 3 (DB3) filter is used. This filter achieves a good compromise between the number of used points and the detail of the filtered scales.

In Fig. 4, the filtering steps in both the coupled and the uncoupled simulations can be seen. From left to right, the columns show the contour plots after filtering once, twice, and three times the results of the significant wave height (H_s). Further filtering was found to not be desirable since NaNs propagate with each filtering step. This figure shows that the coupled simulation has a large number of small structures and also that after the third (DB3) filtering step, these small structures disappear, so by reconstructing the filtered parts the small scales can be quantified.

3. Results

3.1. Atmosphere

3.1.1. Wind speed

The mean velocity had an initial peak at hour 18 (17/01/2020 at 18:00 h) of 8 m/s after reaching a value of 5 m/s at hour 50 and strongly raised to a maximum of 10.2 m/s at hour 68, which was maintained until hour 104. From that moment on, the wind started to decay until hour 152 with a value of 5 m/s, a point that can be considered the end of the storm. Finally, a gentle relaxation was observed until hour 192 (day 25/01/2020) until 3 m/s were reached. Fig. 7 shows the behavior of the non-dimensionalized wind speed.

Table 1 shows some daily and spatially-averaged statistical parameters in relation to wind speed. The locations were classified as coast (C), land (L) and sea (S), as explained in the methodology. The differences

[3] The Network of Automatic Meteorological Stations (XEMA) was created in 1996 and integrates all the automatic meteorological stations managed by the Meteorological Service of Catalonia.

[4] Puertos del Estado is a public agency under the Spanish Ministry of Transport, Mobility and Urban Agenda, with global responsibilities over the entire state-owned harbours system.

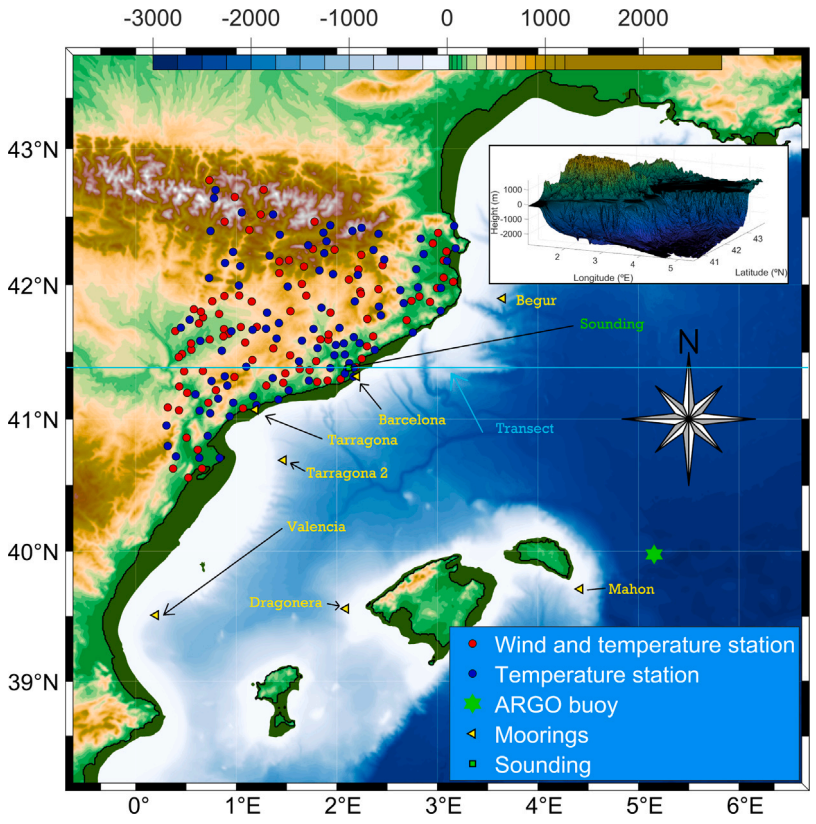

Fig. 3. Map with the location of meteorological stations, moorings, sounding, and ARGO buoy, as well as a surface plot to visualize a fragment of the mesh of WRF and ROMS in the Gulf of Lion area. The cyan line is the transect that will be used to show σ_T in Fig. 9.

between the simulations are minor; the mean and standard deviation showed percentages that in no case exceeded 1.0%. However, when calculating the mean point-to-point differences using the root mean square error (RMSE) (Carvalho et al., 2012; Hyndman and Koehler, 2006), it was observed that the discrepancies were not negligible even during the first day, being similar in the different zones (between 0.56 and 0.65). The RMSE values were higher when the average speed increased (January 20th and 21st for example), while when the wind speed decreases, the differences are also reduced.

As for the mean velocity, the largest values in magnitude and the largest differences in percentage, as well as the largest standard deviations were found at sea. However, the highest RMSEs were found at land locations when the storm was at its peak and afterward. RMSE values were higher in the land region on the 22nd and 23rd of January, and it must be highlighted that they were notably greater than those of the mean velocity. As a consequence, after this period of strong wind, the model differences did not return to the initial values. Furthermore, having a large RMSE and a low mean relative difference implied that the local velocity differences became relatively large even though the overall storm behavior was the same. As can be seen from the RMSE, the velocity variations created at the water sites where data are exchanged in the coupled model propagate inland and are sometimes larger than those generated over the sea itself. For this reason, the coupled simulation can be a good choice not only if most of the domain is water, but also when there is a good balance between sea and land.

Higher magnitudes, larger differences, and higher standard deviations in mean velocity were observed at sea, while the highest root mean square errors (RMSEs) were found in land regions during and after the peak of the storm. These RMSE values remained notably higher than those of the mean velocity, indicating that local velocity differences remained large even though the storm finished.

The XEMA weather stations showed that the differences between the simulations and the weather stations oscillated around 0, with a standard deviation of 1 m/s. These differences increased with higher wind intensity, peaking at 1.5 m/s bias with a standard deviation of 2.5 m/s during the storm, but returned to initial values after the storm.

The differences between the coupled and uncoupled simulations were negligible, indicating that the coupled simulation did not significantly improve the velocity values overall. The scatter plot analysis of time-averaged wind speed (in intervals of 2 m/s) between the models and the stations, showed that 57 stations were between 0 and 2 m/s, 32 stations between 2 and 4 m/s, and 2 between 4 and 6 m/s, only one station in the Pyrenees with more than 6 m/s difference. This suggests that both simulations produced similar results, except for that particular station.

3.1.2. Temperature

Fig. 5, shows the temperature versus height of the storm averaged into three time frames as well as the whole storm, this plot has a wide range of temperatures hence is not possible to distinguish between simulations, but can give an idea of the evolution of the storm in this field. Focusing on the differences of the coupled simulation with respect to the uncoupled one, at the lower elevations (217.3 m) the temperature difference was 0.12 °C at the beginning of the storm, during the storm it was 0.14 °C and at the end of the storm it was 0.22 °C. This showed that the discrepancy, in the end, was greater than during the strong wind episode. At a height of 12067.7 m, the differences were 0.0077 °C, 0.000015 °C, and 0.0033 °C at the beginning, middle, and end of each period respectively. In the upper part, (20262.4 m) the differences were −0.005 °C, −0.0025 °C, and +0.001 °C. The values above show that the differences were greater at the end of the storm and closer to the surface.

According to Table 2, the coupled simulation showed slightly higher temperatures compared to the uncoupled simulation, with a maximum difference of 1.2%. The mean percentage difference varied throughout the days, with higher values in the sea and lower values at the coast

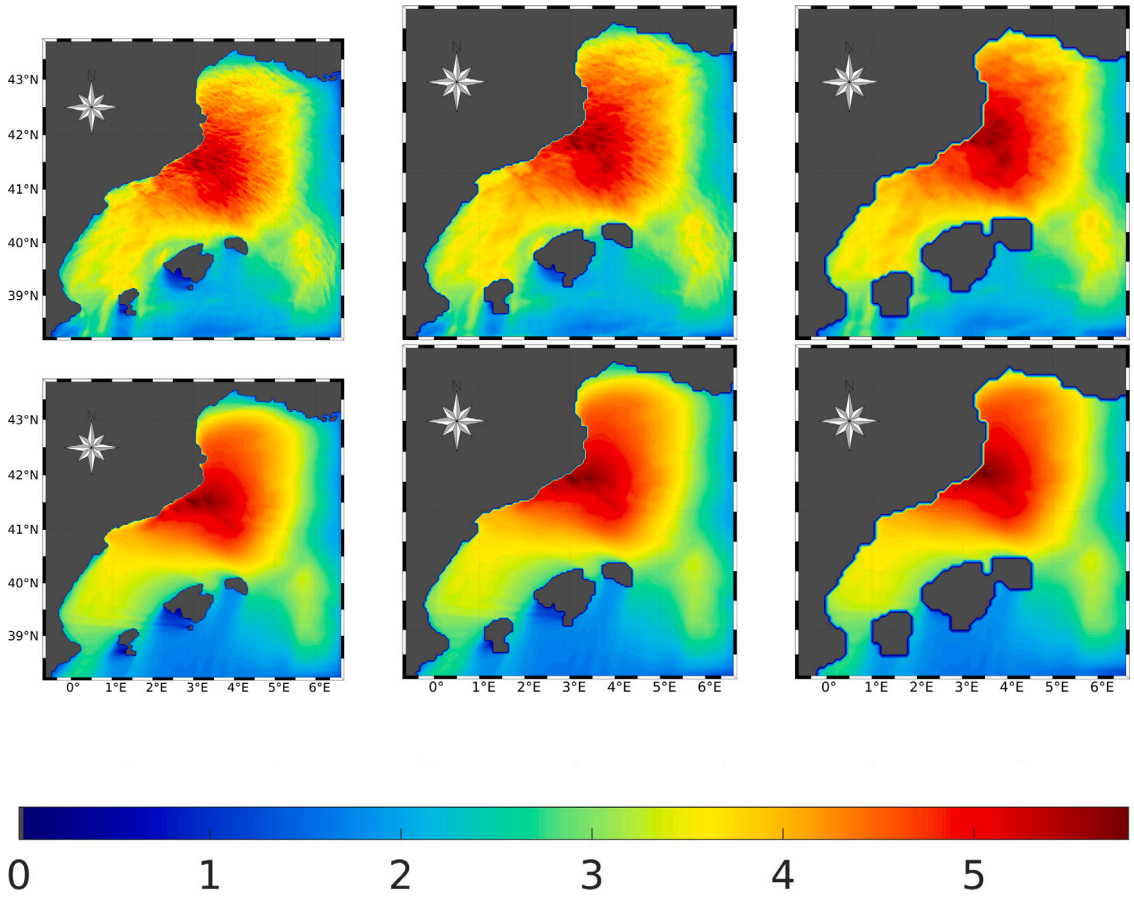

Fig. 4. Contours of the significant wave height (H_s) for the coupled (top) and uncoupled (bottom) simulations, during the filtering process: after the first step (left), the second (middle), and the third one (right) on 22/01/2020 00:00 h.

Table 1
Comparison of wind speed (m/s) statistics between coupled and uncoupled simulations averaged spatially and temporally. Nomenclature: L = land, S = sea, C = coast, Co = Coupled, U = Uncoupled. Mean = Mean Velocity, P = Relative difference (coupled-uncoupled)/coupled, STD = Standard Deviation of Velocity, RMSE = Root Mean Square Error between both simulations.

Day	Zone	Co.Mean	U.Mean	P. Mean (%)	Co.STD	U.STD	P. STD (%)	RMSE
17	S	8.54	8.62	−1.00	2.16	2.16	−0.12	0.56
17	C	4.84	4.88	−0.84	1.69	1.71	−0.79	0.62
17	L	4.29	4.29	−0.18	1.93	1.93	0.00090	0.65
18	S	6.39	6.45	−0.84	2.06	2.10	−0.73	0.49
18	C	3.72	3.73	−0.10	1.31	1.32	−0.49	0.46
18	L	2.81	2.82	−0.12	1.42	1.42	−0.11	0.30
19	S	10.82	10.88	−0.58	3.42	3.43	−0.34	0.81
19	C	8.53	8.52	0.14	2.59	2.60	−0.65	1.14
19	L	4.88	4.89	−0.19	2.16	2.17	−0.55	0.89
20	S	15.01	15.04	−0.21	3.05	3.02	0.74	1.05
20	C	10.62	10.61	0.15	3.13	3.13	−0.22	1.36
20	L	6.06	6.05	0.16	2.47	2.48	−0.27	0.90
21	S	14.76	14.84	−0.57	2.19	2.20	−0.27	1.00
21	C	10.11	10.18	−0.70	2.88	2.91	−0.95	1.35
21	L	5.51	5.48	0.49	2.55	2.56	−0.16	1.25
22	S	10.78	10.82	−0.36	2.78	2.81	−1.15	0.68
22	C	7.22	7.22	−0.0069	2.00	1.98	0.95	0.87
22	L	3.49	3.49	−0.060	1.93	1.95	−0.61	1.08
23	S	6.58	6.64	−0.86	1.85	1.89	−2.22	0.51
23	C	4.61	4.59	0.54	1.29	1.27	1.09	0.59
23	L	2.77	2.77	0.23	1.53	1.53	−0.11	0.84
24	S	4.62	4.65	−0.72	1.57	1.59	−0.94	0.75
24	C	3.06	3.09	−1.13	1.10	1.10	0.36	0.64
24	L	1.85	1.85	−0.03	0.96	0.96	−0.11	0.44

and land on days 17th, 18th, 19th, and 23rd. However, during and after the storm, this pattern shifted, and larger differences were observed in land on the 20th and on the coast on the 20th and 24th. The standard deviation was consistently larger offshore and smaller inland, without

Table 2
Statistic comparison of the temperature at 2 m above ground level (AGL) (°C) between coupled and uncoupled simulations, averaged spatially and temporally. Nomenclature: L = land, S = sea, C = coast, Co = Coupled, U = Uncoupled. Mean = Mean Velocity, P = Relative difference (coupled-uncoupled)/coupled, STD = Standard Deviation of temperature, RMSE = Root Mean Square Error between the temperatures in both simulations.

Day	Zone	Co.Mean	U.Mean	P. Mean (%)	Co.STD	U.STD	P. STD (%)	RMSE
17	S	13.76	13.89	−0.93	0.52	0.52	0.82	0.21
17	C	11.98	12.05	−0.56	1.55	1.57	−1.21	0.30
17	L	7.42	7.42	−0.11	2.09	2.09	−0.15	0.25
18	S	12.91	13.06	−1.20	0.35	0.36	−1.18	0.20
18	C	11.06	11.10	−0.41	1.53	1.54	−1.07	0.21
18	L	6.74	6.75	−0.16	1.73	1.73	−0.16	0.15
19	S	12.17	12.31	−1.15	0.90	0.88	2.19	0.24
19	C	10.03	10.06	−0.29	1.37	1.39	−1.15	0.26
19	L	4.90	4.90	−0.02	2.01	2.01	−0.21	0.23
20	S	12.13	12.26	−1.04	1.20	1.18	1.73	0.27
20	C	9.27	9.33	−0.69	1.38	1.39	−0.82	0.28
20	L	3.41	3.44	−1.10	2.31	2.33	−0.44	0.22
21	S	13.84	13.94	−0.71	0.72	0.73	−1.40	0.22
21	C	11.55	11.63	−0.72	1.26	1.27	−0.75	0.33
21	L	5.99	6.01	−0.22	2.23	2.24	−0.50	0.32
22	S	14.58	14.66	−0.54	0.65	0.69	−5.34	0.22
22	C	12.74	12.76	−0.16	1.23	1.25	−1.52	0.30
22	L	6.97	6.95	0.26	2.20	2.21	−0.82	0.29
23	S	13.98	14.07	−0.59	0.79	0.83	−5.27	0.32
23	C	12.06	12.08	−0.10	1.31	1.32	−0.63	0.28
23	L	6.58	6.57	0.080	2.15	2.16	−0.35	0.29
24	S	12.92	13.03	−0.86	0.87	0.85	2.73	0.56
24	C	10.63	10.74	−1.05	1.43	1.47	−2.49	0.52
24	L	6.06	6.07	−0.26	1.95	1.95	−0.25	0.29

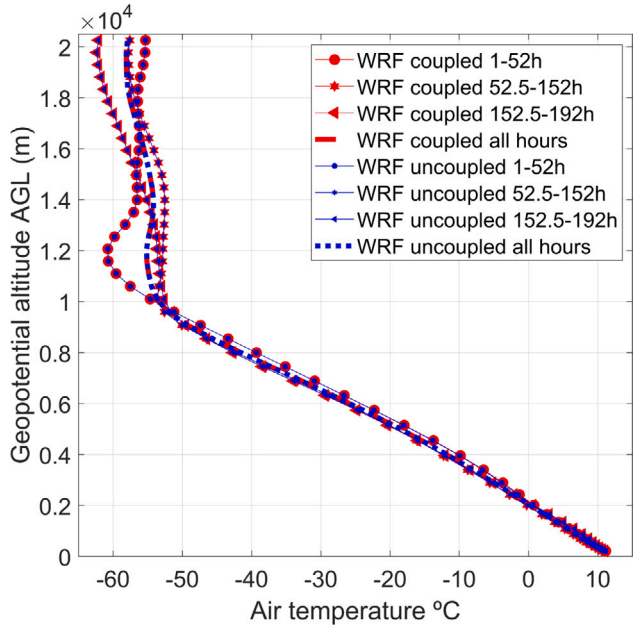

Fig. 5. Plot of temperature versus geopotential altitude of coupled and uncoupled simulations. Red markers are the WRF coupled simulation, and blue markers the WRF uncoupled simulations.

a clear bias towards the coupled or uncoupled simulations. The RMSE increased towards the end of the storm, indicating significant local differences that could be relevant. Before and during the storm, coastal locations had higher RMSE values compared to the other areas, but after the storm, the sea exhibited the greatest differences.

The simulations were compared to experimental data of XEMA stations similar to the velocity fields. The coupling does not have a clear improvement in XEMA locations. The temperature results showed that on certain days (17th, 20th, 21st, and 24th), both simulations had higher temperatures than the stations, while on days 18th and 19th, the temperatures varied between colder and warmer. For the remaining days (22th and 23th), the simulations were very similar to the XEMA. The temperature differences have a maximum of almost 2.5 °C, at the end of the storm. The overall mean difference between the coupled simulation and the stations was 0.46 °C, with a mean standard deviation of 1.89 °C. The uncoupled simulation had similar mean difference and standard deviation values (0.44 °C and 1.89 °C. The atmospheric vertical profiles (Fig. 6 is an example of 19th at 12:00 h) showed good agreement with the model.

3.1.3. Relative humidity

Relative humidity (HR) was compared to the experimental data from XEMA stations. The coupling did not generate a significant difference. This variable experienced important changes over time, but its detailed description is not considered relevant. The STD of RH had an average of 12.79%, but in some moments it increased as in hour 18, where it had a value of 31.34%.

3.1.4. Temporal evolution of differences

The discrepancies between the simulations were primarily attributed to differences in wind speed, with secondary factors like current feedback, SST feedback, and wave height also influencing the results. Although the discrepancies decreased after the storm's peak, they remained higher than the initial values. A daily histogram analysis of the velocity differences between the coupled and uncoupled simulations showed a correlation between the differences and the storm's kinetic energy. The histograms exhibited a widening shape as the velocity magnitude increases. These histograms have not been included because there are a large number of them.

During the first simulated day, the average velocity magnitude (VM) was approximately 2 m/s, and the histograms not included showed a concentration of data points around 0 m/s. Towards the end of the first day, there was a peak in VM prior to the storm, which decreased during the second day. The histograms exhibited a narrow shape on January 17th, which gradually became wider as VM increased. After the peak intensity of the storm, the histograms maintained a wide shape despite VM returning to values even lower than the initial levels. It was observed that following a prolonged period of high velocities, the

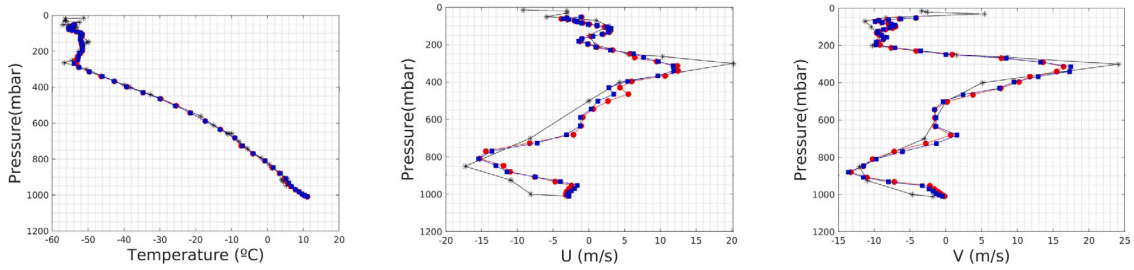

Fig. 6. Vertical profile of temperature (left), U (center) and V (right) wind velocity for coupled (●), uncoupled (●) and observed sounding data (★) from a vertical profile in Barcelona latitude 41.3844°N and longitude 2.1181°E, on the 19th at 12:00 h.

local differences between simulations took time to converge toward the initial values. This phenomenon can have significant implications for long-duration simulations.

In Fig. 7, the analysis compares RMSE variations in coupled and uncoupled simulations for different surface variables. Discrepancies do not indicate correctness or incorrectness; they demonstrate the impact of the coupling on the model. This applies throughout the article, except when comparing with experimental data. The RMSE values were normalized with the corresponding mean in order to compare them. Moreover, normalized VM was used as a reference variable. This figure reaffirms the conclusions obtained in the previous analyses.

The temperature did not show a significant variation during the simulation and slightly increased at the end. The RMSE of the horizontal velocity, (U and V in the legend of Fig. 7 with blue and cyan colors) had a medium sensitivity to the average storm velocity (black solid line). PBL seemed to have a higher sensitivity to increases and changes in the VM. Finally, the most affected variable, as expected, was the vertical velocity which can be related to changes in density due to the different SST which is one of the coupling variables among other factors. Additionally, in this figure, the differences between hours 48 and 192 can be appreciated. Both have a very similar velocity magnitude, although the normalized RMSE of all the variables is higher at the end of the storm. This means that the differences in the studied variables caused during the storm are propagated in time.

3.2. Ocean

The ROMS ocean model and the Simulation WAves Nearshore (SWAN) were used and evaluated to compare the results of the coupled and uncoupled simulations.

3.2.1. Ocean currents

The forcing of the atmospheric model on the ocean model was one of the main sources of energy input, so it was expected to see significant variations once the coupling was activated. The differences are shown in Fig. 8, represented in the four subzones into which the domain was divided (Fig. 2). In zone 1, Fig. 8 shows that the difference between the coupled and uncoupled model velocities was larger than in the other zones, where the mean depth was lower. The mean depths were −1020.8 m, −1892.3 m, −2694.1 m, and −1300.5 m in zones 1, 2, 3, and 4 respectively.

Zone 1 have a combination of strong winds, shallow waters, and a large speed channel formed between the Balearic archipelago and the coast. These factors caused the average current speed to double the value of the other zones. The comparison between the models showed the greatest differences when the kinetic energy of the storm was bigger. The maximum differences between currents in zones 1, 2, 3 and 4 were 0.65 m/s, 0.18 m/s, 0.17 m/s and 0.15 m/s respectively. The average wind speed in zone 1 was also higher than in the other zones (3 m/s).

The surface stresses had similar behavior, but surprisingly, the differences between models were smaller in zone 1 than in the rest even though the surface velocity magnitude values were larger. The maximum values in zones 1, 2, 3, and 4 were respectively 1.14 Nm^{-2}, 0.82 Nm^{-2}, 0.68 Nm^{-2} and 0.78 Nm^{-2}. Apart from this, the differences in temperatures between models were smaller in zone 1 (see below). Hence, the changes observed between models could not be attributed to the wind intensity, but were based on the interaction of all coupling variables like current–wave interaction and the frequency of coupling (6 min instead of 1 h).

Furthermore, this Fig. 8 includes the difference between the coupled and uncoupled simulation of the angle formed by the currents and stresses in each zone. It can be observed that in zones 1 and 4, there is a significant difference in angles between the simulations when the storm intensity is higher. However, this effect is not evident in zones 2 and 3. Therefore, although this difference has an effect on the magnitude of the velocity, it is not the main cause that explains the differences in the velocity magnitude between simulations.

3.2.2. Temperature

Temperature presented a sinusoidal evolution in every zone. This was due to the daily frequency which corresponded to the effect of the solar radiation parameters and the influence of the storm itself. The peaks appeared in the early afternoon, around 3 pm. The coupled model reached a maximum temperature of 14.46 °C on the 17th, and a minimum of 14.12 °C on the 24th day. In the case of the uncoupled simulation, the behavior was similar, but values were slightly lower and so were peak variations, around 0.01 °C. The mean differences between coupled and uncoupled simulations were 0.12 °C, 0.24 °C the maximum difference, and 0.04 °C the minimum one which was obtained at hours 160 and 17, respectively. The lower temperature of non-coupled simulations during a cyclone event is explained in Jin et al. (2009).

The low-frequency wave went from the initial value to a minimum of 14.12 °C at hour 79 of the simulation and then increased to a value of 14.45 °C at hour 160, and this was only observable in zone 2 at the north-east of the domain. Table 3 showed the daily statistics of the different zones, where it can be seen that the differences were bigger in zones 1, 3, and 4 near the Balearic archipelago, and that zone 2 was the one with lower differences almost every day. At the end of the simulation, zone 3 and 4 had a bigger increase in temperature difference.

In the Table 3, interesting differences between RMSE and average speed evolution could be observed. For example in zone 1 on day 17th the difference of the value was 0.16 °C and reached a value of 0.066 °C on 21st which was almost 2.5 times less. The RMSE went from 0.13 °C to 0.18 °C in the same periods, and this behavior was repeated in all the zones. Therefore, the mean value difference between coupled and uncoupled could be reduced significantly, but the RMSE difference was more stable. At the end of the simulation zones 3 and 4 were the ones where the model discrepancies became higher.

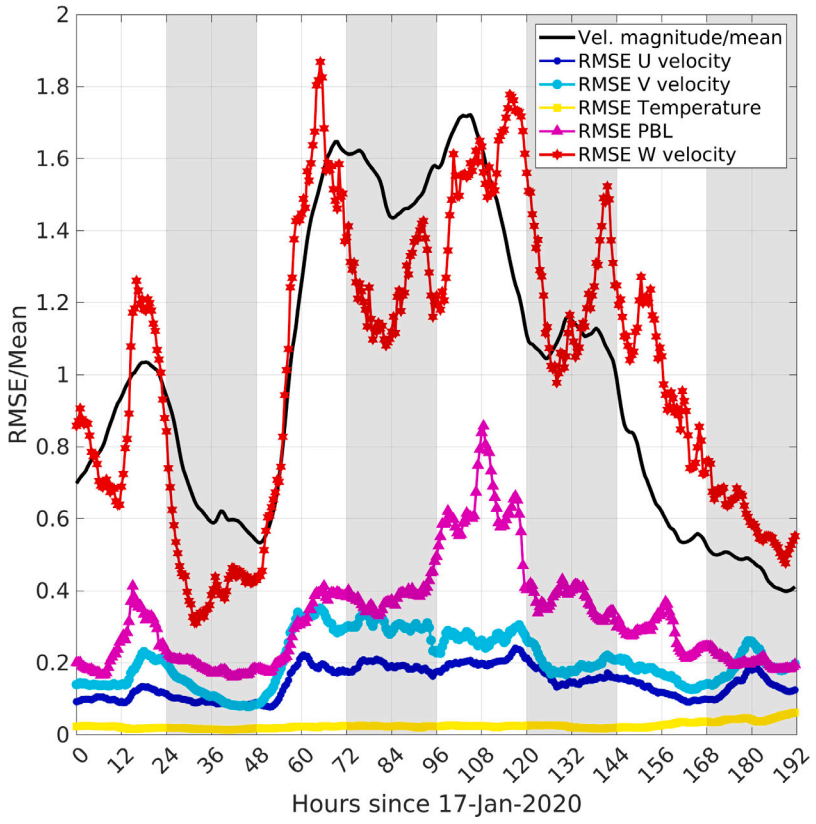

Fig. 7. Plot of the root mean square error (RMSE) of different variables calculated in the uncoupled simulation with respect to the coupled one, normalized with the mean of the absolute value obtained in the coupled simulation. The black line (—) is the normalized velocity modulus, which is used to compare the behavior of the variables with wind intensity. $U10$(●) and $V10$ (●) are the longitudinal and latitudinal components of the wind, respectively, both referred to 10 m height. W(✱) is the vertical component of the velocity at an average height of 48.43 m. Temperature (★) is taken at 2 m height, and PBL (▲) represents the height of the planetary boundary layer. All variables are spatially averaged over the entire domain. Gray stripes helps the readers to separate days.

Table 3
Comparison of temperature (°C) statistics between coupled and uncoupled models averaged spatially and temporally. Where, DM = difference of mean value (coupled - uncoupled), RMSE = Root Mean Square Error between the temperature of both models, Z = zone.

Day	DM Z1	DM Z2	DM Z3	DM Z4	RMSE Z1	RMSE Z2	RMSE Z3	RMSE Z4
17	0.16	0.10	0.15	0.16	0.18	0.13	0.16	0.17
18	0.17	0.10	0.15	0.16	0.19	0.15	0.16	0.17
19	0.13	0.079	0.12	0.11	0.17	0.13	0.13	0.13
20	0.13	0.076	0.11	0.12	0.20	0.17	0.13	0.15
21	0.066	0.076	0.10	0.15	0.11	0.17	0.13	0.17
22	0.080	0.078	0.15	0.18	0.11	0.15	0.18	0.20
23	0.15	0.11	0.21	0.25	0.18	0.16	0.23	0.27
24	0.19	0.14	0.26	0.28	0.22	0.18	0.27	0.30

3.2.3. Salinity

The coupling had a low impact on the salinity field, with a slightly greater influence observed at the free surface compared to the seafloor. This conclusion was drawn from analyzing salinity in three spatial dimensions and its temporal evolution.

To provide reference values, the average salinity at the free surface in the entire domain was examined. On the 17th at 00:00 h, the uncoupled and coupled models had average values of 13.72 and 13.74, respectively. These values remained nearly constant for two days, with a slight decrease to 13.72 and 13.74 on the 20th and 21st. The salinity then remained constant on the 22nd, and on the 23rd, there was a very small increase, resulting in a reduction of the difference between the models. Salinity decreased on the 24th, reaching a value of 37.75 in both models.

The variation of RMSE with height was also studied. An exponential fitting was applied, resulting in the equation $y = 0.01612\exp(0.03463x)$. This fitting exhibited a high correlation coefficient ($R^2 = 0.978$).

3.2.4. Thermocline

The depth of the thermocline plays a fundamental role in hurricanes and was expected to play a relevant role in the case of a strong storm event as well. In this study, the thermocline was defined as the depth where the vertical temperature gradient was maximum. The thermocline average was calculated in two different ways: over time and over space, and then both calculations were compared.

The time-averaged analysis showed similar large structures, but some pathological zones could be detected, in general surrounding the islands. The greatest differences were found in the south of the islands of Mallorca and Ibiza, as well as somewhat smaller differences between the islands and the Valencian coast. The differences averaged over the whole time series were 4.02 m, 1.68 m, 1.68 m, and 2.98 m in zones 1, 2, 3, and 4 respectively. The zones 1 and 4 (located near the coast and the archipelago) were those where the coupling had the strongest effect, while the Gulf of Lion and the southeast of the domain, where the differences were smaller.

In general, the thermocline showed the greatest difference at 3 pm, coinciding with the temperature differences, which is expected since

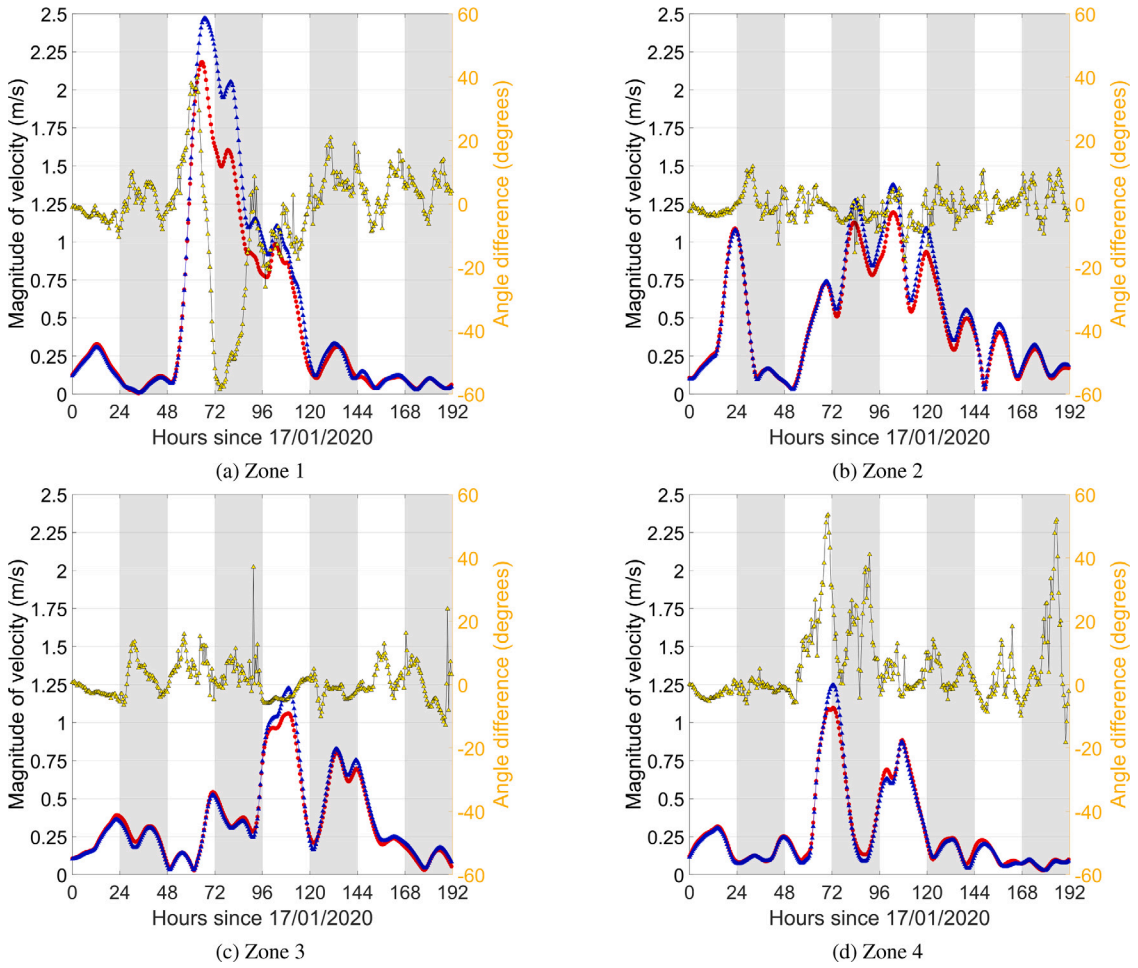

Fig. 8. Spatial average of ocean current magnitude (m/s) in the four domain zones. Coupled (●), uncoupled (▲) and angle difference (△) (which is the difference between the coupled and uncoupled simulation of the angle formed by the currents and stresses).

the thermocline and temperature are strongly related. During the storm, as the wind speed increased, the differences became smaller. Initially, differences could reach up to 6 m, but on the 19th and 20th, they were less than 0.3 m. On the 21st, the maximum difference was 0.9 m, which increased to approximately 3.5 meters at the end of the storm. Overall, the coupled model exhibited a shallower thermocline depth. Solar radiation played a role in this, as it heated the water during the early afternoon, resulting in a peak in the thermocline. The warmer surface reduced the maximum temperature change by a few meters. It should be noticed that the radiation flux in the uncoupled simulation was also hourly exchanged, from the uncoupled WRF simulation data, and so were the pressure, clouds, rain, relative air humidity, pressure, and horizontal wind velocity. The radiation flux coupling is important not only in the case of a strong storm but also during anticyclones or other calm periods.

3.3. Cross sections

Vertical slices or transects of temperature, salinity, and density were studied, in three different locations: Gulf of Lion, Barcelona, and Palma, and at two different times: at hour 102 (21st 06:00 h) when the storm was at its peak, and at hour 192 when the storm ended. Data were taken for the coupled and uncoupled simulations to study their differences. Most changes were observed in the first 500 m. For temperature and density, the greatest differences occurred within a few meters from the free surface, depending on currents, weather, and bathymetry, among other factors. See as an example, the plots in Fig. 9 for σ_T density ($\sigma(S,T) - 1000$ kg m^{-3}) at the peak and the end of the storm.

In the case of σ_T density, there was a factor of three in the difference between the two methods between the middle and the end of the storm. Salinity and temperature had smaller differences in some cases, like in Barcelona where the factor was two. The case of Palma had similar behavior, except from one point close to a longitude of 6.5°, where the difference was bigger at the end of the storm.

3.3.1. Bathymetry-based analysis

The temperature at maximum storm intensity showed no significant differences between the coupled and uncoupled simulations, and this occurred in all depths. In the first 50 m, the temperature difference had a maximum value of 0.32 °C and a minimum of 0.075 °C. Between 50 and 200 m depth, the maximum and minimum values were 0.27 °C and 0.075 °C, respectively. All horizontal points deeper than 200 m had differences ranging from a maximum of 0.24 °C and a minimum of 0.076 °C. The differences reached their maximum during midday (generally at 15:00 h).

Salinity showed the following behavior: from 0 to 50 m, it had a constant difference of 0.02 during the first two days, the third day presented small oscillations around this value, then it increased slightly during 2 days until it reached a maximum of 0.06 at approximately 112 h. At the end of the storm, it drastically decreased to a value of 0.005 at 132 h, and then it raised almost linearly with small oscillations until the difference reached a value of 0.06.

From 50 to 200 m, it had values from 0.005 to 0.01 during approximately the first 48 h. In this case, the tendency was equal to that of less than 50 m, and values were similar except for some specific cases where a significant difference could be observed. In hour 92, it reached

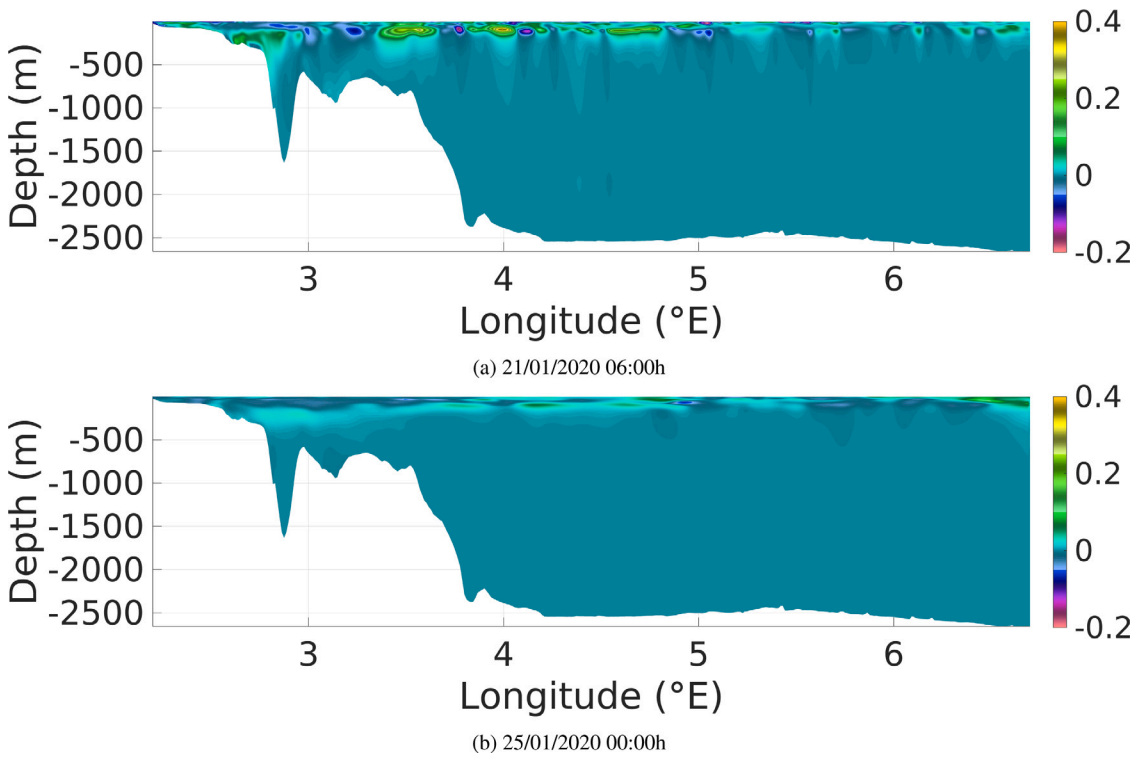

Fig. 9. Transect of σ_T density differences between coupled and uncoupled simulations at different instances in time in the Barcelona latitude (41.3865°N).

Table 4
Comparison of simulations for the best fit data of temperature at the mooring buoys. Equal means that it was not clear which one was better.

Day	Barcelona	Dragonera	Tarragona	Tarragona 2	Valencia
17	COUPLED	COUPLED	COUPLED	COUPLED	COUPLED
18	COUPLED	COUPLED	COUPLED	COUPLED	COUPLED
19	COUPLED	UNCOUPLED	COUPLED	COUPLED	COUPLED
20	NO DATA	COUPLED	COUPLED	COUPLED	COUPLED
21	NO DATA	EQUAL	EQUAL	EQUAL	COUPLED
22	NO DATA	COUPLED	EQUAL	EQUAL	COUPLED
23	NO DATA	COUPLED	COUPLED	NO DATA	COUPLED
24	NO DATA	COUPLED	COUPLED	NO DATA	COUPLED

a value of 0.05 being two and a half times higher than in the first 50 m. In hour 132, it had an approximate value of 0.05, while from hour 144 onwards it had an almost-constant value of 0.03 until the end of the simulation.

At a depth of more than 200 m, during the first three days, it had a constant value of 0.01. During the first 5 h of the fourth day, the difference increased to 0.024, and this value was maintained for approximately 24 h. Then, it gradually decreased to 0.4 at the end, and in this decay, small oscillations were observed.

3.3.2. Comparison with experimental data

To compare model results with observations, the mooring buoys data from *Puertos del Estado* were used. These are in Barcelona, Dragonera, Tarragona (2 moorings) and Valencia. Table 4 was used to assess the best simulation in terms of temperature for the given experimental data, considering the temperature of the mooring as the true value and the difference between both simulations with the moorings. In general, the coupled one was better at capturing the ocean observations, as in the case of Valencia where the differences were large, in Dragonera the coupled one was still better, although not during all days (In supplementary materials 5.2.1 the plots of the mooring are shown).

3.3.3. Satellite vs. models comparison

Satellite data consist of daily data for the sea surface temperature (SST) (Copernicus, 2022) from Copernicus (Merchant et al., 2019), with Level-4 spatially complete global SST product based on data from multiple sensors at 0.05° grid resolution.

These values were interpolated to the points in the domain using the dispersion interpolation method and plotted along the results from coupled and uncoupled simulations in Fig. 10. Both coupled and uncoupled simulations showed good agreement with the satellite data, the coupled one was slightly better with a warmer SST. At the end of the storm, the decoupled simulation showed an excess of cooling. The SST values of the coupled one fell within the uncertainty range of the satellite data at all times, whereas the decoupled SST was outside the uncertainty range on Jan 17th, 18th, 23rd, and 24th. When considering the standard deviation of the simulations, the SST could be validated. It must be highlighted that the maximum difference between the mean of the satellite data and the uncoupled simulation was 0.4 °C, and only 0.1 °C if the uncertainty of the satellite was considered.

3.3.4. Significant wave height

In this section, the significant wave height (H_s) was studied using the SWAN model. H_s was defined as the mean wave height from the trough to the crest of the highest third of the simulated waves.

Fig. 11 shows H_s and its range in both simulations, by considering the standard deviations (color shades). The maximum difference (see green line) between them occurred at hour 84 (when compared with the coupled model the relative difference was 11%, and it was 10% when compared with the uncoupled one), as in the other previously-explained fields, the difference increased with the magnitude of the wind speed.

Despite ROMS and WRF, this difference declined to a value close to zero at the end of the storm, which can be explained by the fact that waves need less than 24 h to cross the domain, as confirmed by separate tests.

For some time steps, there were appreciable differences in the small-scale structures. An analysis of the auto-correlation of H_s (not

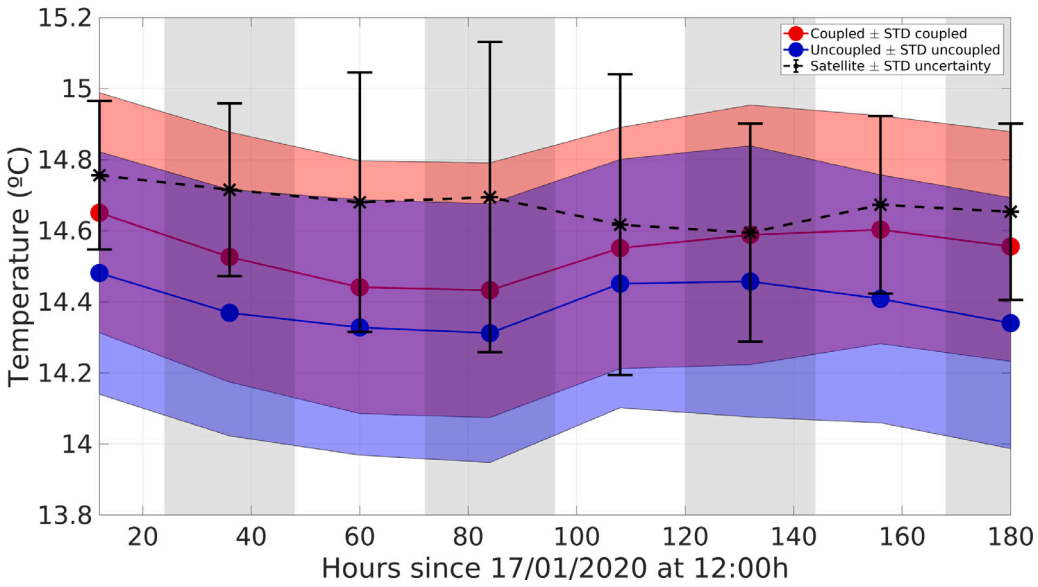

Fig. 10. Values of sea surface temperature (°C) from both simulations and satellite data. Color shades stand for the corresponding standard deviation of the model predictions, and the bars for the satellite data uncertainty, coupled (●), uncoupled (●).

included here) showed that in the coupled simulation the correlation of small structures decayed slightly faster. Therefore, a more precise method for the quantification of this difference, which was based on wavelet analysis, was performed. Fig. 12 shows the wavelet (DB3) decomposition explained in 2.2.4. It was evaluated by incorporating the absolute values of significant wave height of the filtered parts. Each of them was divided by the maximum in order to normalize them. In the beginning, both simulations showed the same amount of filtered H_s, but the coupled one was much more sensitive to changes in wind intensity. Additionally, at the end of the storm, the filtered signal of the coupled simulation had more small scales captured by the filter.

3.3.5. Mooring buoys and models comparison

Both simulations were compared with the mooring buoys of *Puertos del Estado*. Both showed a good agreement with experimental observations. In the case of Begur and Mahon, there was a greater difference during the most intense part of the storm than the rest of it, but the trends of all lines were the same. Unlike the uncoupled one, the experimental data tended to oscillate as in the coupled one. However, the uncoupled simulation showed a better agreement in two cases, Begur and Valencia as depicted in Fig. 13.

3.3.6. Correlation of ocean and atmosphere

Pearson's Linear Correlation Coefficient for wind and current velocity from coupled and uncoupled simulations was used. The correlation between the atmosphere and the ocean, in each simulation, shows variations in currents caused by coupling and is independent of the overall magnitude of velocity fields, disregarding the energy dissipation effect caused by SWAN, for example. Therefore, this value reflects changes in the current direction between simulations. Once the correlation of coupled and uncoupled was calculated, the differences between them were determined and plotted, as can be seen in Fig. 14 for both components of the velocity. This figure highlights that both components of velocity had similar values and their difference oscillated around zero. Still, the spatial correlation difference of the V component of velocity was more susceptible when the wind was stronger, and these oscillating differences resulted in small changes in directions.

The eddy kinetic energy (EKE) in the atmospheric model (WRF) was not appreciably different when the two methodologies were compared. Hence, it was not included here. The ocean (ROMS) EKE showed some differences instead. These were summarized in Table 5, where the slope of the regression line in the different periods was reported.

Table 5
Values of the mean, maximum, and slope of the regression line over time, extracted from the EKE differences between the coupled and uncoupled method, normalized for the ROMS model.

Hours	Mean	Max	Slope
0–57.5	−0.0024	0.00462	0.000033
58–71.5	0.13	0.31	0.024
72–88.5	0.21	0.31	−0.011
89–136.5	0.069	0.14	−0.0020
137–192	0.0060	0.014	−0.00019

The slope values denoted an absence of variability in the beginning, a large increase from hour 58 to 71.5, followed by a steady decrease until hour 88.5, then, a smoother decrease, and finally another zone of no variability. The lateral forcing conditions were the same for both simulations, and the only difference was the forcing condition coupled with WRF. The maximum difference of 31% in the EKE showed an important energy reduction when the storm was intense, but it was not so significant before and after the storm occurred.

4. Discussion and conclusions

4.1. Discussion

The COAWST model was implemented in the northwestern Mediterranean Sea to study the storm Gloria. It was validated using experimental data from satellites, moorings, ARGO buoys, and weather stations. Moreover, a qualitative comparison was performed using operational model outputs from METEOCAT. The main objective of this study was to provide information about the predictive value of coupled and uncoupled simulations in high-energy events. This study has certain limitations. Only one storm has been studied from its formation until shortly after its conclusion, so the long-term behavior during periods of low energy has not been addressed. Additionally, while some differences can be explained with the performed analysis, in other cases, it would be necessary to perform simulations by deactivating parameterizations one by one to precisely evaluate their individual effects. For example, in the SWAN model, simulating the non-coupled model with current forcing and another with a coupling time of 1 h would be necessary to ensure what causes the differences at small scales. However, due to the high computational cost of these simulations, such

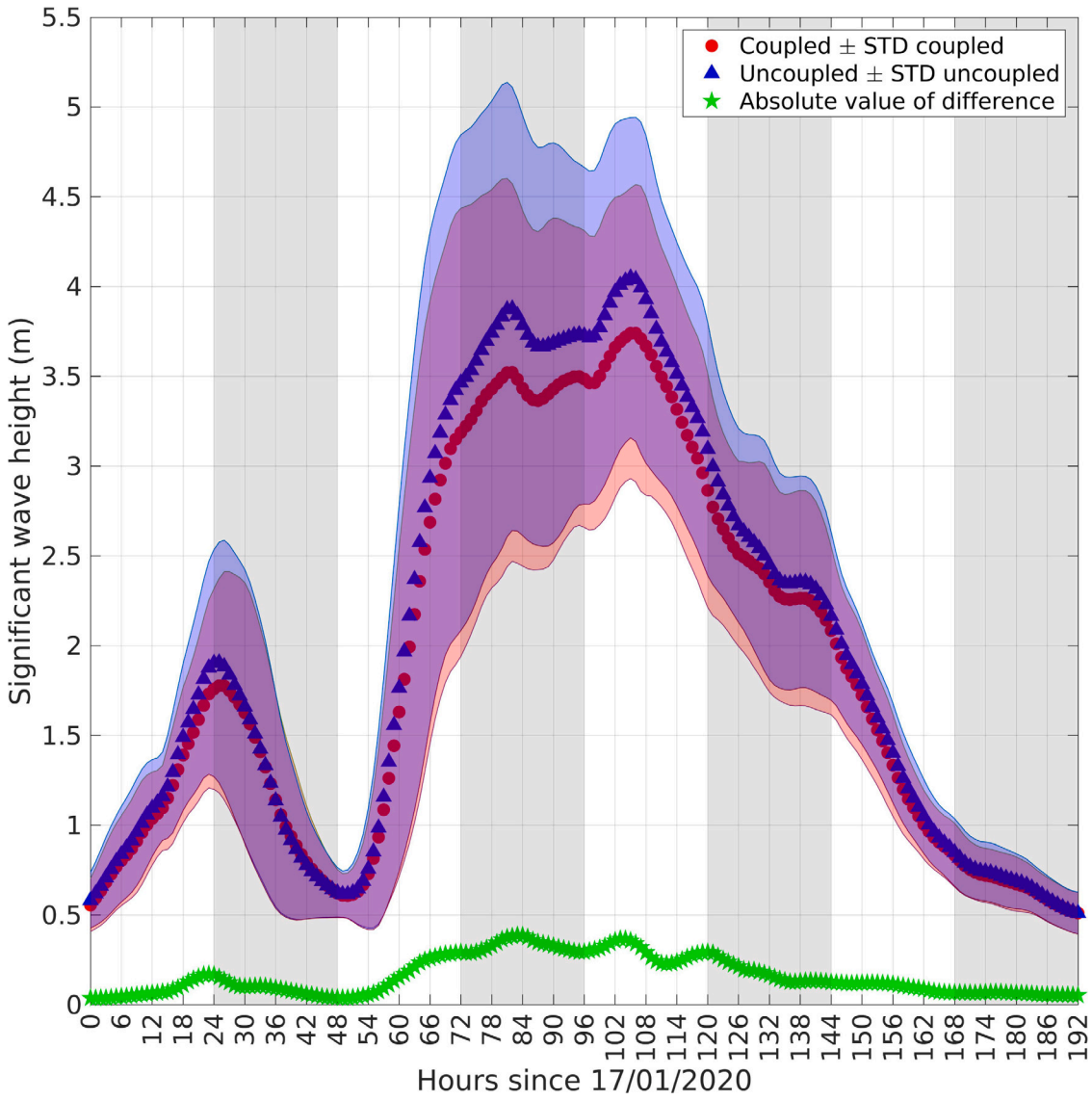

Fig. 11. Comparison of the spatially averaged significant wave height (H_s) between coupled(●), uncoupled (▲) and with their respective standard deviations in a shade zone and the absolute value of the point-to-point differences (★), also spatially averaged.

an analysis is not feasible for all studied variables. The results of this work were briefly compared with two other similar studies. The first one, from De Alfonso et al. (2021), does a reanalysis of the Gloria storm. Fig. 4 of the cited article plots the evolution of H_s from the PORTUS-wana reanalysis model for four buoys: Dragonera, Valencia, Tarragona (inshore), and Begur. In the case of Dragonera, both studies, the De Alfonso et al. (2021) and the present one showed an almost perfect match with the experimental data. However, in the case of Valencia and Tarragona, the PORTUS model overestimated H_s while the present study underestimated it. Finally, in Begur the PORTUS model showed a better agreement than this study, where H_s was underestimated. As the PORTUS-wana reanalysis uses variable forcing and resolution (Table 2 of the cited reference), it was difficult to explain the differences observed between both works. A possible explanation is the resolution. In the cited reference, the forcings were taken from Aemet with 1,152 × 864 grid points and 2.5 km horizontal resolution, covering the whole Iberian Peninsula and the Balearic Islands. Despite employing different models (PORTUS/SWAN) and different forcing conditions (AEMET/WRF), both achieved good agreement with the moorings except at the Begur buoy.

Unlike this work, the second article (Renault et al., 2012) analyzed a similar domain but was focused on how the coupling and the different ways of interaction between the coupled models (WRF, ROMS and SWAN) improved storm modeling. Moreover, the Gloria storm had a greater impact and was stronger in terms of storm intensity than those analyzed in the cited reference. It used a nested grid of 27.9 and 3 km in WRF, whereas ROMS and SWAN ran on a single grid with a horizontal resolution of ~1.8 km and 30 σ levels.

The comparison, in this case, was based on some considerations since the present study analyzed a different storm. In the work of Renault et al. it was observed that despite the physics of the storm being well reproduced, the wind speed and H_s tended to be higher in the decoupled simulation. This phenomenon was also observed in the present work, but without overestimating the values since they were closer to the real ones in the area of the experimental observations. It must be taken into account that the different parameterizations of the schemes, resolution, etc. may affect the outcome. In the present work, it was also seen that the coupling affected vertical mixing as mentioned in the thermocline analysis.

Some studies (see introduction) conclude that inter-model feedback in coupling had negative effects. This could be explained by the horizontal spatial resolution. In those studies, the resolution was around three times lower than the present one. That is, in this work, there

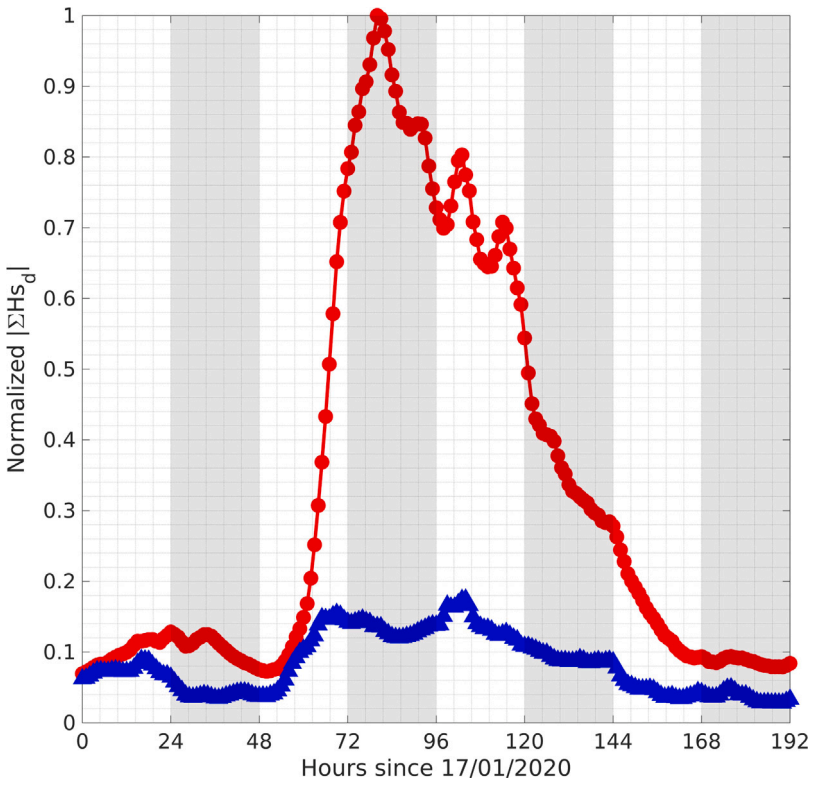

Fig. 12. Time evolution of the sum of the filtered significant wave height H_s obtained by applying the Daubechies 3 wavelet filter three times, for both the coupled (●) and uncoupled (▲) simulations.

is at least a ratio of 9:1 grid points, with respect to the studies that report a negative performance. It is therefore advisable to first make a study of the coupled simulation in the region of interest, especially if a high-resolution grid is affordable.

In this study, it was found that the coupled and uncoupled simulations perform similarly in spatial averages of wind, temperature, PBL, etc., but the analysis of small structures showed some differences (e.g., see Table 1). The results for temperature and velocity in the coupled and uncoupled ones agreed well with the weather station data, and atmospheric profiles, but the differences increased when the storm had more kinetic energy. The distribution of stations with larger differences was not concentrated in a specific area: in 62% of the stations, the time-averaged difference was less than 2 m/s with respect to the results of both simulations. Regarding temperature, the differences between simulations as a function of altitude were greater at the surface, while at medium or high altitudes the changes could be neglected.

The zone analysis of temperature at 2 m height, showed that depending on the location (land, sea, or coast) the coupling did not have a significant overall effect in terms of spatially averaged temperature. Still, the RMSE values experienced some small-scale changes that increased at the end of the storm.

In addition, changes in the sea region were propagated to the coast and land, especially when wind speed was high. When the wind speed was lower, both the coupled and uncoupled simulations gave similar values, and if eventually, the wind increased, then the agreement between both simulations recovered. Still, if the increase occurred over a longer period, such as 48 h, then both cases differed appreciably. The differences became smaller as the storm intensity decreased, but remained higher than before the start of the storm.

It was not possible to distinguish the best-performing simulation in the WRF model with the available data from the meteorological stations, as both showed similar results at these locations. The relative humidity in both was similar to the observations, except for some specific hours where both simulations differed equally from the experimental data. The PBL height was highly dependent on wind speed but did not show significant discrepancies between the simulations at the end of the storm. The vertical W component of the velocity, closely related to the kinetic energy behavior, was the variable that showed the largest differences. This can be explained by the fact that the SST is exchanged in the coupled simulation, which changes the air density and hence the vertical velocity. In this work, the resolution of 48 vertical layers is not sufficient for a detailed study of vertical velocity.

The mean current and mean sea surface temperature from ROMS showed significant differences between the coupled and uncoupled simulations. The coupled one provided a lower average velocity and a higher average temperature when the storm was in its most energetic period. However, the overall differences become almost negligible after the storm ends, although the point-to-point mean difference was still important.

The analysis of the thermocline showed some significant differences between the two cases. During calm periods, a sharp decrease in thermocline depth was observed during midday due to the variation in the superficial temperature, but it was lower in the uncoupled method.

Vertical slices of temperature, density, and salinity showed that most of the differences were found in the first 500 m, and their magnitude was related to the intensity of the storm. Temperature and density showed differences greater than salinity. The bathymetric analysis of temperature showed how in the first layers the difference was greater than in the deeper ones. When the storm was more intense, the mixing decreased this difference.

The mooring buoy data showed good agreement with both simulations but were better in the coupled case. The satellite SST agreed better with the coupled simulation results for all days. In summary, all the experimental data showed better agreement with those from the coupled simulation, so the coupled simulation was considered a better approximation to the real ocean conditions.

The significant wave height in SWAN differed between both simulations (coupled and uncoupled) when the wind was stronger, but unlike

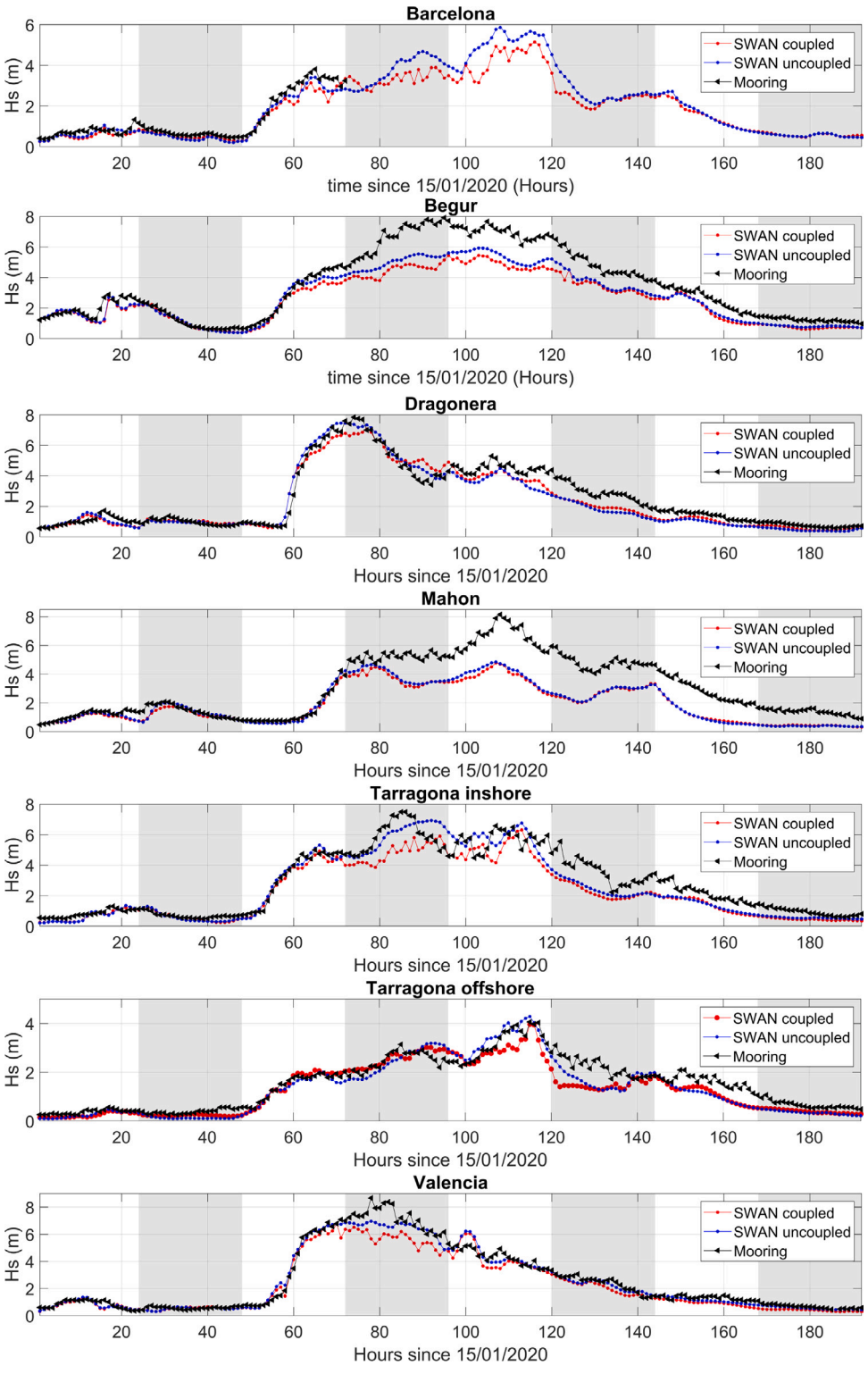

(a) 22/01/2020

Fig. 13. Significant wave height (H_s) for both simulations of SWAN model. Compared to the mooring buoys at different locations, coupled (●), uncoupled (●) and mooring (●)

the WRF and ROMS, the difference at the end decreased faster. Both simulations obtained similar large structures, although the significant wave height values were larger in the uncoupled one. However, the small structures differed.

The wavelet analysis of H_s showed that the amount of small scales in the coupled simulation was much bigger than in the uncoupled one and that it was affected by the forcing conditions. At the end of the storm, the difference between them in terms of small scales was larger than in the beginning. The data from both cases had the same shape and trend as those from the moored buoys. In two of the buoys the uncoupled simulation obtained results closer to the experimental ones, but without capturing the oscillating behavior.

The reduction of H_s and the richness of fine structures in the coupled simulation can be attributed to two factors. Firstly, the interaction

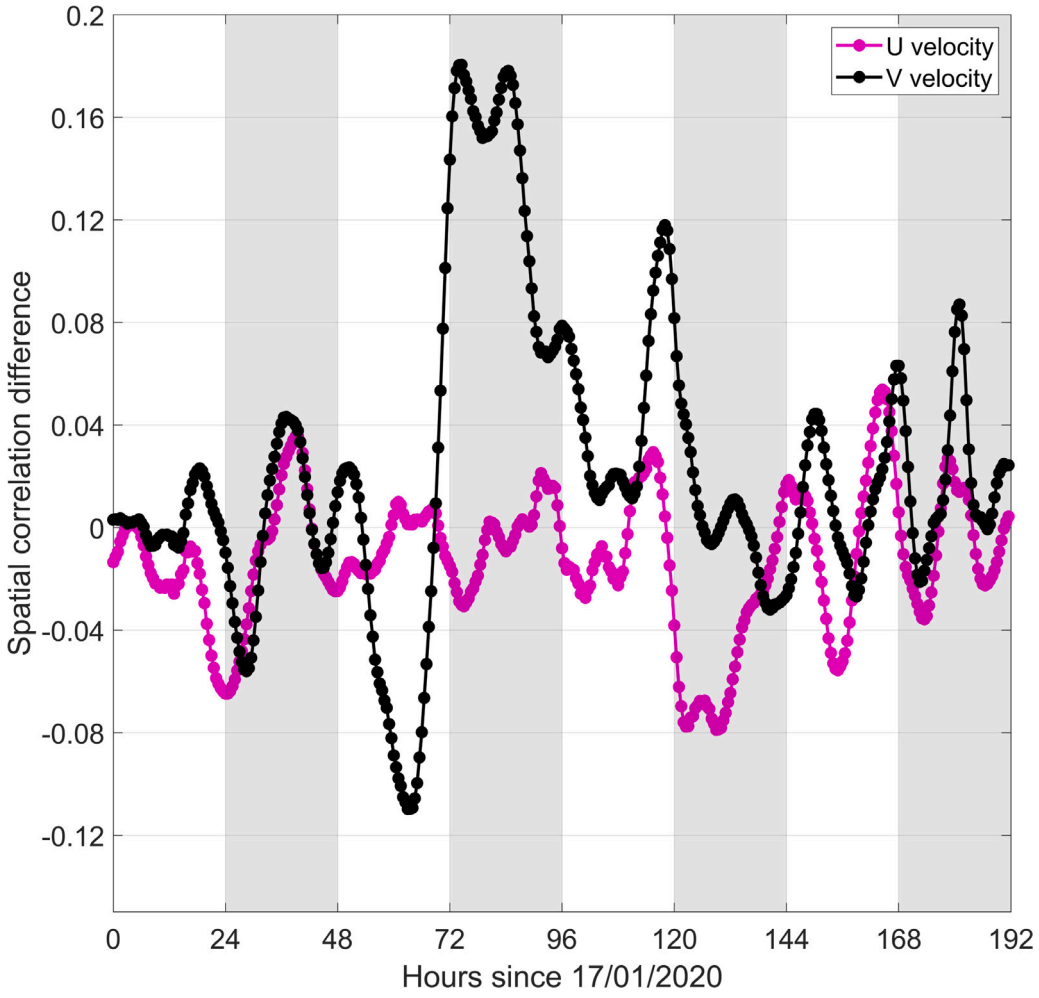

Fig. 14. Difference of the spatial correlation over time. Positive values are when the coupled simulation had a bigger correlation between the atmospheric and ocean model. Negative values are when the uncoupled shows better correlation, The correlation was performed with U (●) and V (●) velocities, separately.

between currents and waves is only forced in the coupled simulation. In a study by Bôas et al. (2020), it was found that the spatial variability of Hs is highly sensitive to the nature of the underlying current, resulting in gradients of Hs. Secondly, in the decoupled simulation, the forced wind inflow condition was updated every hour, whereas in the coupled simulation, it was updated every three minutes. Smaller changes in the wind allowed the creation of larger waves. This is because the wind blew in the same direction for a longer time, so the contact angle between the wave and the wind increased and the force was optimized, generating larger waves.

The study of computational times and numerical efficiency of the different simulations is beyond the scope of this paper. However, without detailed study, there is no significant difference in computational times, the wave model is less efficient and is the bottleneck, but it is compensated because in the non-coupled simulation, the models must be run sequentially and post-processed in order to prepare the inputs for the ocean models.

4.2. Conclusions

The coupled simulation presented a series of advantages during the storm with respect to the uncoupled one in special the oceanic models. The coupled mode of simulation does not have a large impact on the atmospheric model when compared to data available from meteorological stations or atmospheric soundings. Moreover, at the end of the storm, the RMSE of the difference between simulations was higher in velocity, temperature, etc., as explained in the corresponding sections which can result in significant differences in longer simulations. Ocean and wave models show significant differences in temperature, velocity, H_s, and other variables, and experimental data confirm that coupling has a beneficial effect.

One of the objectives of this work is to define under which conditions coupled simulations have advantages over uncoupled simulations. The atmospheric model has been studied in coastal areas, at sea, and inland, and as explained the differences occur at sea during periods of low storm intensity but are transmitted to coastal and land areas, especially when the intensity is high.

The oceanic results show significant differences and these occur mainly in the first 500 m, where there is more mixing and the velocities are higher. The experimental data of temperature, show a better agreement with the coupled simulation. The atmosphere–ocean correlations show a higher correlation in the V component of the velocity with the coupled simulation during the most intense part of the storm. However, outside this high-intensity period, the differences in the atmosphere–ocean correlations between simulations are significantly smaller and are not biased towards either the coupled or the uncoupled simulations. In addition, the normalized EKE differences show an increase at the beginning of the storm, decreasing as the storm progresses, and almost completely vanishing at the end of the storm. Finally, the wave model captures better the small oscillations of H_s in the coupled simulation compared to the buoys, with the drawback that momentum is lost in the wind speed and H_s is underestimated in the coupled simulation.

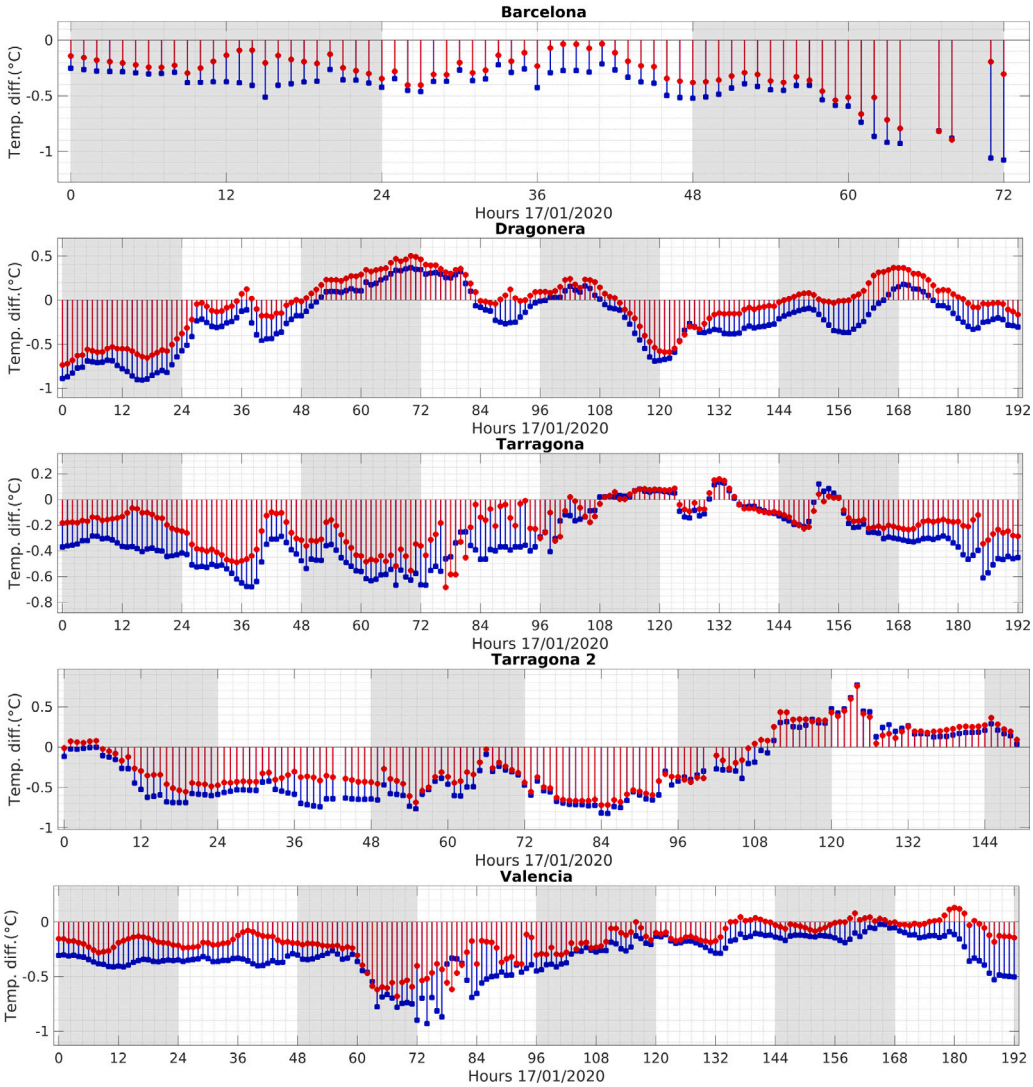

Fig. 15. Temperature difference for both simulations, coupled (●) and uncoupled (■).

5. Supplementary material

5.1. Software

5.1.1. Atmospheric model

The Weather Research and Forecasting (Skamarock et al.) is a model developed by National Center for Environmental Prediction and National Centers for Atmospheric Research among others. This model is non-hydrostatic, quasi-compressible, and has a variety of parameterizations concerning the atmospheric boundary layer, the mesoscale and microscale of motion, and so on. It uses a third-order Runge–Kutta scheme, along with acoustic schemes. The mesh is Arakawa-C grid, the vertical coordinates are sigma hybrid that follow the terrain close to it and turn the pressure levels in the upper layers. The model is able to predict three-dimensional wind momentum, surface pressure, precipitation, etc.

5.1.2. Oceanic model

Regional Ocean Modeling System (Shchepetkin and McWilliams, 2005)is a free code written in F90/F95. It uses a C-preprocessing in order to activate the various physical and numerical options and the code, like the other two, can be used in parallel. ROMS is a three-dimensional model with free surface, it is discretized with vertical sigma coordinates and solves primitive equations. The turbulence modeling uses Reynolds Average Navier–Stokes equations; it is a hydrostatic model and operates with Boussinesq approximation. The hydrostatic momentum equations have a split time step scheme, where barotropic and baroclinic modes are solved separately. The mesh is discretized horizontally with a staggered grid using Arakawa-C discretization and vertically the coordinates are terrain following with stretching near the surface.

5.1.3. Wave model

The Simulation WAves Nearshore (Booij et al., 1999) used in the COAWST configuration is a spectral wave model specific for coastal areas or shallow water. The model estimates wave parameters like wave propagation refraction due to current and depth, frequency shifting, whitecapping, dissipation due to aquatic vegetation, etc, from given wind, bottom, and current conditions.

5.2. Models details

In all three models the mesh has the same horizontal geographic points, with no nested domains. This was intentionally defined to avoid differences when interpolating the data between different coordinates, as well as in the boundary zone in the nestings, where the solutions are not smooth across the boundaries of the nested domains. The

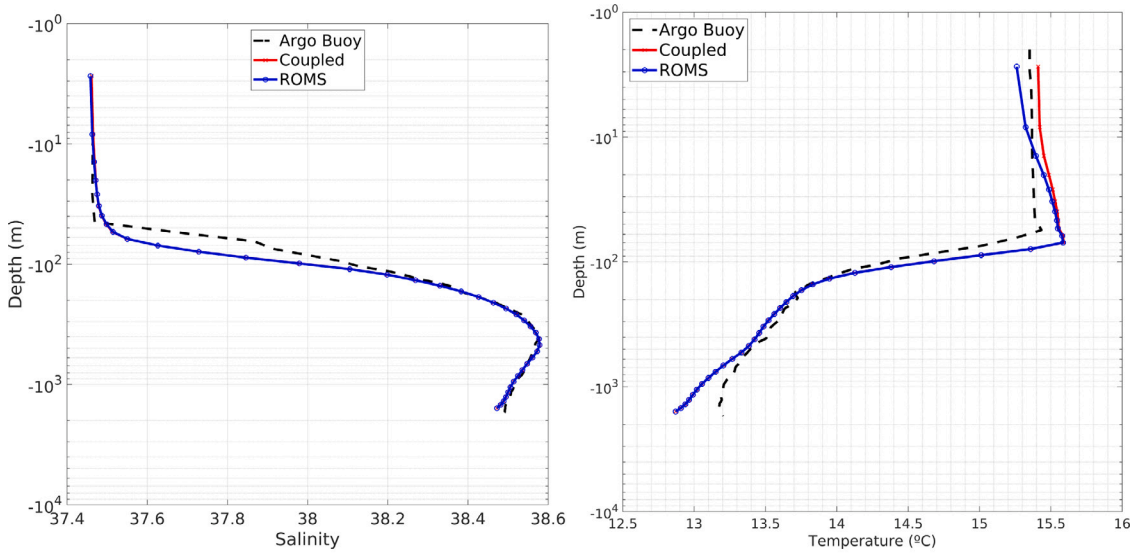

(a) Salinity (b) Temperature

Fig. 16. ARGO buoy in longitude 5.1555 and latitude 39.9752 on 23 Jan 2020 at 05:45 h the data was compared with 06:00 h.

three models have a Mercator projection, and horizontal resolution of 649 × 649 rho points, considering rho point the center of each cell. In the case of the atmospheric model, the prognostic fields are calculated up to the stratosphere, with a maximum height of 20311 m over the sea level, divided into 47 rho points.

The parameterizations used are, 5 class schemes from microphysics, Yonsei University Scheme for Planetary Boundary Layer, Kain–Fritsch Scheme for cumulus, Dudhia Shortwave Scheme and RRTM Longwave Scheme for shortwave and longwave respectively, 5–layer Thermal Diffusion Scheme for land surface, Revised MM5 Scheme for the surface layer The timestep is 6 s, following the recommendation of six times the distance between cells. Some other time steps were tested in order to evaluate the model stability, if it is larger the Courant–Friedrichs–Lewy (CFL) becomes too high; a vertical dumping was also used.

The oceanic model has 649 × 649 × 40 rho points, the advection scheme is 3rd-order upstream-biased in horizontal and 4th-order centered differences in vertical. The closure parameters for turbulence modeling of k-epsilon are used. The distance between mesh cells is 1 km in horizontal, while vertically is variable depending on the zone. Sigma coordinates are used with stretching near the surface. All single-cell bays were eliminated and replaced by two water cells, or none, depending on the most similar case with the real coastline. ROMS uses the CMEMS hourly input data, as mentioned above, using a five-cell nudging to update the model for each hourly boundary feed, as is done in the WRF model. The nudging forcing is relaxed by a function as it deepens. The SWAN configuration uses third generation KOMEN, whitecapping, and the BSBT scheme.

The domain was created in the following way: first the static geographic data from WPS (UCAR) was used for thirty seconds. Then, the mesh was cloned for use in ROMS. To avoid a single cell bay in ROMS, some shore points were modified, as well as others that were improved relative to the actual shoreline. Variables such as land usage, albedo, height, etc, were also adapted to these changes. In the case of height, the value was that of the mean of the adjacent cells, in the case of land use and other categorical variables, the mode of the surrounding cells was assigned. Once the ROMS mesh was adapted to the most realistic scenario, the bathymetry was implemented. It was obtained from EMODnet database, with an spatial resolution of 1/16 arcminute in square grid implying approximately 115 km between cells. The mesh stiffness was adapted following the Hanley criterion (between 0 and 0.4) as well as Beckmann & Haidvogel criterion (between 3 and 7). Cells that did not meet both criteria were modified iteratively, until the entire grid met these conditions. Once the ROMS mesh was completed, the SWAN mesh was created using the same landmask and bathymetry, and finally, the modified points in the ROMS model were also changed in the WRF geologic mesh. Because if there were inconsistencies in the models, i.e. if there were cells defined in ROMS as land, but set in WRF as sea, the temperature would not be exchanged. Then WRF would use a static value for sea surface temperature inconsistent with that of adjacent cells.

5.2.1. *Mooring buoys*

Fig. 15 shows the temperature difference plots for the model and the mooring buoys at the different locations, a positive value means that the model is warmer than the buoy.

5.2.2. *Argo buoys*

Argo buoys were also used in the analysis to compare the simulations with actual experiments. Only 18 of the buoys are available for this period within the domain, and many of these values are either unreasonable or missing. Because of this unforeseen difficulty, only the analysis of one of the buoys (see Fig. 16), located at 39.9752N, 5.1555E on 23 Jan 2020 at 5:45 h AM, was shown. These data were compared with those from the simulations at 6AM. The buoy height was calculated using Eqn.(3.32.3) from IOC et al. (2010) –the height in simulation data is not 0 m because the temperature is at the center of the rho cell in sigma coordinates.

CRediT authorship contribution statement

Jordi Iglesias: Conceptualization of this study, Methodology, Software. **Ildefonso Cuesta:** Data curation, Writing – original draft. **Clara Salueña:** Data curation, Writing – original draft. **Jordi Moré:** METEOCAT data supply, Editing. **Jordi Solé:** Data curation, Writing – original draft.

Declaration of competing interest

The authors declare that they have no known competing financial interests or personal relationships that could have appeared to influence the work reported in this paper.

Data availability

Data will be made available on request

Acknowledgments

This work has been funded by Spanish Ministerio de Ciencia, Innovación y Universidades through the grant PID2020-113303GB-C21 (MCIU/AEI/FEDER, UE), by the Generalitat de Catalunya through the grant 2017-SGR-1234 and by Universitat Rovira i Virgili through the grant 2019PMF-PIPF. The authors thank the Copernicus Marine Environment Monitoring Service (CMEMS) and Puertos del Estado for data publicly available, and the Servei Meteorològic de Catalunya (METEOCAT) as well as CMEMS for additional supplied data and outputs of their models which were a crucial part for this work.

Appendix A. Supplementary data

Supplementary material related to this article can be found online at https://doi.org/10.1016/j.envsoft.2023.105830.

References

Amidror, I., 2002. Scattered data interpolation methods for electronic imaging systems: A survey. J. Electron. Imaging 11 (2), 157–176.

Amores, A., Marcos, M., Carrió, D.S., Gómez-Pujol, L., 2020. Coastal impacts of storm Gloria (January 2020) over the north-western Mediterranean. Nat. Hazards Earth Syst. Sci. 20 (7), 1955–1968.

Barbariol, F., Benetazzo, A., Carniel, S., Sclavo, M., 2013. Improving the assessment of wave energy resources by means of coupled wave-ocean numerical modeling. Renew. Energy 60, 462–471.

Bôas, A.B.V., Cornuelle, B.D., Mazloff, M.R., Gille, S.T., Ardhuin, F., 2020. Wave–current interactions at meso-and submesoscales: Insights from idealized numerical simulations.

Booij, N., Ris, R.C., Holthuijsen, L.H., 1999. A third-generation wave model for coastal regions: 1. Model description and validation. J. Geophys. Res.: Oceans 104 (C4), 7649–7666.

Carvalho, D., Rocha, A., Gómez-Gesteira, M., Santos, C., 2012. A sensitivity study of the WRF model in wind simulation for an area of high wind energy. Environ. Model. Softw. 33, 23–34.

Clavel-Henry, M., Solé, J., Ahumada-Sempoal, M.-Á., Bahamon, N., Briton, F., Rotllant, G., et al., 2019. Influence of the summer deep-sea circulations on passive drifts among the submarine canyons in the northwestern Mediterranean sea. Ocean Sci. 15 (6), 1745–1759.

Clavel-Henry, M., Solé, J., Bahamon, N., Carretón, M., Company, J.B., 2021. Larval transport of aristeus antennatus shrimp (crustacea: Decapoda: Dendrobranchiata: Aristeidae) near the Palamós submarine canyon (NW Mediterranean Sea) linked to the north balearic front. Prog. Oceanogr. 192, 102515.

Commission, I.O., et al., 2015. The International Thermodynamic Equation of Seawater–2010: Calculation and Use of Thermodynamic Properties.[Includes Corrections Up to 31st October 2015]. UNESCO.

Copernicus, 2022. Copernicus. https://cds.climate.copernicus.eu/cdsapp#!/dataset/satellite-sea-surface-temperature?tab=overview, Accessed: 2022-09-01.

De Alfonso, M., Lin-Ye, J., García-Valdecasas, J.M., Pérez-Rubio, S., Luna, M.Y., Santos-Muñoz, D., Ruiz, M.I., Pérez-Gómez, B., Álvarez-Fanjul, E., 2021. Storm gloria: sea state evolution based on in situ measurements and modeled data and its impact on extreme values. Front. Mar. Sci. 8, 270.

Delbeke, 2022. The impact of the war in Ukraine on Europe's climate and energy policy. https://www.eui.eu/news-hub?id=the-impact-of-the-war-in-ukraine-on-europes-climate-and-energy-policy, Accessed: 2022-09-15.

Domingues, M.O., Mendes Jr., O., da Costa, A.M., 2005. On wavelet techniques in atmospheric sciences. Adv. Space Res. 35 (5), 831–842.

ECMWF, 2022. Using copernicus data to track volcanic sulphur dioxide emissions. https://www.copernicus.eu/en/news/news/observer-using-copernicus-data-track-volcanic-sulphur-dioxide-emissions, Accessed: 2022-09-15.

Ekström, M., 2016. Metrics to identify meaningful downscaling skill in WRF simulations of intense rainfall events. Environ. Model. Softw. 79, 267–284.

Hyndman, R.J., Koehler, A.B., 2006. Another look at measures of forecast accuracy. Int. J. Forecast. 22 (4), 679–688.

IPCC, 2022. Climate change 2007 synthesis report. https://www.ipcc.ch/site/assets/uploads/2018/02/ar4_syr_full_report.pdf, Accessed: 2022-10-13.

Jin, X., Dong, C., Kurian, J., McWilliams, J.C., Chelton, D.B., Li, Z., 2009. SST–wind interaction in coastal upwelling: Oceanic simulation with empirical coupling. J. Phys. Oceanogr. 39 (11), 2957–2970.

Le Roux, R., Katurji, M., Zawar-Reza, P., Quénol, H., Sturman, A., 2018. Comparison of statistical and dynamical downscaling results from the WRF model. Environ. Model. Softw. 100, 67–73.

María Palomares, A., Navarro, J., Grifoll, M., Pallares, E., Espino, M., 2016. Application of a wind-wave-current coupled model in the Catalan coast (NW Mediterranean sea), for wind energy purposes. In: EGU General Assembly Conference Abstracts. In: EGU General Assembly Conference Abstracts, EPSC2016–1202.

Merchant, C.J., Embury, O., Bulgin, C.E., Block, T., Corlett, G.K., Fiedler, E., Good, S.A., Mittaz, J., Rayner, N.A., Berry, D., et al., 2019. Satellite-based time-series of sea-surface temperature since 1981 for climate applications. Sci. Data 6 (1), 1–18.

Millot, C., 1999. Circulation in the western Mediterranean sea. J. Mar. Syst. 20 (1–4), 423–442.

Mughal, M.O., Lynch, M., Yu, F., McGann, B., Jeanneret, F., Sutton, J., 2017. Wind modelling, validation and sensitivity study using weather research and forecasting model in complex terrain. Environ. Model. Softw. 90, 107–125.

Nakken, M., 1999. Wavelet analysis of rainfall–runoff variability isolating climatic from anthropogenic patterns. Environ. Model. Softw. 14 (4), 283–295. http://dx.doi.org/10.1016/S1364-8152(98)00080-2, URL https://www.sciencedirect.com/science/article/pii/S1364815298000802.

Nicholls, S.D., Decker, S.G., 2015. Impact of coupling an ocean model to WRF nor'easter simulations. Mon. Weather Rev. 143 (12), 4997–5016.

Ornes, S., 2018. How does climate change influence extreme weather? Impact attribution research seeks answers. Proc. Natl. Acad. Sci. 115 (33), 8232–8235.

Peña, J., Aran, M., Cunillera, J., Amaro, J., 2011. Atmospheric circulation patterns associated with strong wind events in Catalonia. Nat. Hazards Earth Syst. Sci. 11 (1), 145–155.

Pinot, J.M., Tintoré, J., Gomis, D., 1995. Multivariate analysis of the surface circulation in the balearic sea. Prog. Oceanogr. 36 (4), 343–376.

Renault, L., Chiggiato, J., Warner, J.C., Gomez, M., Vizoso, G., Tintoré, J., 2012. Coupled atmosphere-ocean-wave simulations of a storm event over the Gulf of Lion and Balearic Sea. J. Geophys. Res.: Oceans 117 (C9).

Renault, L., Masson, S., Arsouze, T., Madec, G., Mcwilliams, J.C., 2020. Recipes for how to force oceanic model dynamics. J. Adv. Modelling Earth Syst. 12 (2), e2019MS001715.

Renault, L., McWilliams, J.C., Masson, S., 2017. Satellite observations of imprint of oceanic current on wind stress by air-sea coupling. Sci. Rep. 7 (1), 1–7.

Shchepetkin, A.F., McWilliams, J.C., 2005. The regional oceanic modeling system (ROMS): A split-explicit, free-surface, topography-following-coordinate oceanic model. Ocean Model. 9 (4), 347–404.

Skamarock, W., Klemp, J., Dudhia, J., Gill, D., Barker, D., co-authors. 2008. Descr. Adv. Res. WRF Version 3, 1Á113.

Solbakken, K., Birkelund, Y., Samuelsen, E.M., 2021. Evaluation of surface wind using WRF in complex terrain: Atmospheric input data and grid spacing. Environ. Model. Softw. 145, 105182.

Warner, J.C., Armstrong, B., He, R., Zambon, J.B., 2010. Development of a coupled ocean–atmosphere–wave–sediment transport (COAWST) modeling system. Ocean Model. 35 (3), 230–244.

Zambon, J.B., He, R., Warner, J.C., 2014. Investigation of hurricane ivan using the coupled ocean–atmosphere–wave–sediment transport (COAWST) model. Ocean Dyn. 64 (11), 1535–1554.